

LANDAU THEORY OF THE STRUCTURAL PHASE
TRANSITION IN ANTIFERROMAGNETIC CuFeO_2

MARIATHAS JUDES TAGORE



Landau Theory of the Structural Phase Transition in Antiferromagnetic CuFeO_2

by

©Mariathas Judes Tagore

B. Sc (1994) University of Jaffna

M. Math (2002) University of Waterloo

*A thesis submitted to the School of Graduate Studies
in partial fulfillment of the requirement for the Degree of
Master of Science in Physics*

Department of Physics and Physical Oceanography
Memorial University of Newfoundland

St. John's

Newfoundland, Canada

April 2008

Abstract

A Landau-type free energy model is developed to explain experimental ultrasonic velocity measurements on the magnetoelectric compound CuFeO_2 (provided by Dr. G. Quirion at Memorial University) characterizing its low-temperature structural and magnetic phase transitions.

In the first part of this thesis, we investigate the elastic properties of this compound in the neighbourhood of the magnetic and structural phase transitions at 11 K and 14 K. The goal is to understand the measured temperature dependence of the elastic constants of CuFeO_2 . In the high-temperature rhombohedral $\bar{R}3m$ phase, we observe that the elastic constant C_{66} shows a strong softening. This softening behavior is also non-linear. Our Landau model reproduces key features of the data and we therefore can conclude from our studies that the structural transition at 14 K is pseudoproper ferroelastic. The crystal structural symmetry changes from the high-temperature rhombohedral $\bar{R}3m$ to lower-temperature monoclinic $C2/m$ at this structural transition. This work has recently been published ([1] G. Quirion, M.J. Tagore, M.L. Plumer and O.A. Petrenko, *Phys. Rev. B* **77**, 094111 (2008)).

In the last part of this thesis, we examine the impact of the magnetoelastic coupling. First, we develop a Landau model free energy which depends only on magnetic degrees of freedom (the spin density). Analysis shows that there are two magnetic phase transitions at T_{N1} and T_{N2} , coincident with anomalies in the ultrasound data. Second, we analyze a Landau model free energy which contains spin, elastic, and magnetoelastic coupling energy. We again obtain the temperature dependence of three of the six independent elastic constants of CuFeO_2 and demonstrate strong effects due to

spin-lattice coupling.

Dedication

I dedicate this work to my mother Thavamanidevi Mariathas, my father Arulappu Mariathas and my wife Vicky.

Acknowledgements

I wish to express my great appreciation to my supervisor Professor Martin Plumer for his encouragement, moral support, frequent advice, unbelievable patience and helpful discussions and suggestions throughout my program.

I extend my deepest thanks to my co supervisor Professor Guy Quirion for his advices and time spent with me to learn more about Mathematica programming usage and allow me to modify and use his Mathematica programming codes. I also thank him for providing his experimental data of ultrasonic sound velocity measurements on CuFeO_2 to analysis my theoretical model.

I sincerely acknowledge the School of Graduate Studies and Department of Physics and Physical Oceanography to their financial supports. I would like to say thank you to all staff members at the Department of Physics and Physical Oceanography for their kindness and great helps. My special thanks to Fred Perry for his assistance related to the software problems.

I am also grateful to my wife and my parents for their eternal love, emotional support and encouragement during this program.

It is my great pleasure to thank my friends and well - wishers who directly or indirectly encouraged and helped me in the M.Sc. program and contributed to this dissertation, especially to Jason Mercer for his all assistances related to the programming problems.

Contents

Abstract	ii
Acknowledgements	v
List of Tables	viii
List of Figures	ix
1 Introduction	1
2 Elastic Theory	5
2.1 Geometrical Interpretation of strain.	8
2.2 Equilibrium Conditions.	9
2.3 Elastic Constants.	12
2.4 Elastic Energy in Distorted Media.	13
2.5 Crystals	16
2.6 Elastic Energy	17
2.7 Elastic Waves	18
2.7.1 Brief Note about waves	18
2.7.2 Elastic Waves in an Infinite Crystal:	19
3 Landau Theory of Phase Transitions.	25
3.1 Brief Introduction	25
3.2 Role of Symmetry.	26

3.3	Landau free energy for the simplest case of one order parameter: Even order invariants of the order parameter	28
3.3.1	Second Order Transitions: 2-4 potential	30
3.3.2	First Order Transitions: 2-4-6 potential	30
3.4	2-3-4 Potential: Landau free energy for simplest case of one order parameter.	32
4	Landau Free Energy Analysis of Ultrasonic Data on the Ferroelastic $R\bar{3}m \rightarrow C2/m$ Transition in $CuFeO_2$.	34
4.1	Brief Introduction	34
4.2	Ferroelastics and Ferroelastic Transitions	36
4.3	Landau Free Energy for the $R\bar{3}m \rightarrow C2/m$ Ferroelastic Transition in $CuFeO_2$	37
4.4	Derivation of the Model	38
4.5	Effective Elastic Constants	42
4.6	Experimental Results	44
4.7	Numerical Calculation and Model fitting to Ultrasonic Experimental Data on $CuFeO_2$	48
4.7.1	Numerical Calculation	48
4.7.2	Summary of the calculation and model fitting of the data	49
5	Magnetoelastic Coupling	54
5.1	Spin Energy	54
5.1.1	Theoretical Approach	54
5.1.2	Numerical Calculation	59
5.2	Effect of the Magnetoelastic Coupling	61
5.2.1	Numerical model calculation and its prediction	64
6	Conclusions	68
	Bibliography	70

List of Tables

2.1	Polarizations and expressions ρv^2 for velocities for Trigonal ($R\bar{3}m$) Crystals	23
2.2	Polarizations and and expressions ρv^2 for velocities for Monoclinic ($2/m$) Crystals. Note that we are using a coordinate system with the twofold symmetry axis parallel to \hat{x} , not the conventional setting of twofold symmetry axis parallel to \hat{z}	24
4.1	Cartesian coordinate representations of the order parameters and the corresponding transformations under space group generators	38
4.2	Strains under the generators	39
4.3	Effective elastic constants for both phases of CuFeO_2	45
4.4	Expression of ρv^2 for trigonal and monoclinic phases	46
4.5	Velocity values at $T = 300 \text{ K}$	48
4.6	Elastic Constants at $T = 300 \text{ K}$	50
4.7	Coupling/other constants	50
4.8	Strains (S) and order parameters (OP) values at $T = 0 \text{ K}$	50
4.9	Other values: mass density, critical temperature.	50
5.1	Effective elastic constants for both phases of CuFeO_2 as a function of S	65
5.2	Values of coupling constants (LQ and QQ)	66

List of Figures

1.1	(a) Crystal structure of CuFeO_2 . Only Fe^{3+} magnetic ions are shown. (b) Temperature (T) versus magnetic field (B) phase diagram of CuFeO_2 with B applied along the c - axis [7, 8, 9].	2
2.1	Lattice positions before the force action [12].	5
2.2	Lattice positions under the force \mathbf{F} [12].	5
2.3	Elastic distortion [12].	7
2.4	Elastic distortion: 2 D view [13].	8
2.5	Equilibrium forces [12].	10
3.1	Order parameter as a function of temperature. Plot (a) represents a first order transition, here Q decreases to zero discontinuously at T_c . Plot (b) represents a second order transition, Q decreases to zero continuously at T_c [15].	27
3.2	(a) Represents the $R\bar{3}m$ space group structure (Trigonal), (b) represents $C2/m$ space group structure (Monoclinic) [19].	28
3.3	Free energy F_L is a function of the order parameter Q for various values of temperature T . The minima occur at the equilibrium values of Q for each T [15].	31
3.4	(a) Variation of the non-equilibrium potential F_L as a function of temperature, (b) Temperature dependence of the order parameter [15]. . .	32
3.5	Variation of the non-equilibrium potential F_L as a function of temperature [15].	33

4.1	Experimental values for the elastic constant C_{66} as a function of temperature for CuFeO_2	35
4.2	Structural phase transition in CuFeO_2 : $R\bar{3}m$ represented by solid lines and $C2/m$ represented by broken lines [31].	41
4.3	Normalized Velocity Plots: (a) $\Delta V_{Lx}/V_{Lx}$ (C_{11}), (b) $\Delta V_{Tx}(P_y)/V_{Tx}(P_y)$ (C_{66}), (c) $\Delta V_{Lz}/V_{Lz}$ (C_{33}), (d) $\Delta V_{Tx}(P_z)/V_{Tx}(P_y)$ (C_{44}) - We are using a different scale for each plot in order to show the good compatibility of the model and data.	47
4.4	Plot of the order parameter Q_2 , equation (4.6)	51
4.5	Temperature dependence of the strains. Plots correspond to the equation (4.6): (a) $e_p = \frac{e_1 + e_2}{2}$, (b) $e_m = \frac{e_1 - e_2}{2}$, (c) e_3 , (d) e_4	52
5.1	Spin-exchange paths J_1 , J_2 and J_3 within an FeO_2 layer (in plane) and spin-exchange path J' between adjacent FeO_2 layers (planes) [34].	57
5.2	Plot of the free energies for incommensurate and commensurate phases. F_{IC} , and F_C represent the equations (5.30) and (5.32), respectively.	60
5.3	Rescaled temperature dependence of the magnetic moment according to equation (5.33).	62
5.4	Normalized Velocity Plot: $\Delta V_{Lz}/V_{Lz}$. Red curve represents the mean field result and blue curve represents the non-mean field.	66
5.5	Normalized Velocity Plots: (a) $\Delta V_{Ly}/V_{Ly}$, (b) $\Delta V_{TyPz}/V_{TyPz}$ - We are using a different scale for each plot in order to show the good compatibility of the model and data fit.	67

Chapter 1

Introduction

Geometrically frustrated antiferromagnetic systems have recently attracted considerable attention, due to their magnetic and multiferroic (ferromagnetic and ferroelectric) properties [2, 3]. Recent studies show that these types of materials can exhibit the novel magnetoelectric effect under a modest magnetic field. In such systems, it is found that an applied electric field induces a magnetic response and under a magnetic field it shows an induced electric polarization. The magnetoelectric effect is thought to be due to strong magnetoelastic coupling, which couples the lattice and magnetic moments. Some materials have two types of transitions at the same time, which are magnetic and structural transitions. CuFeO_2 is one of these classes of compounds, which we are going to study in this thesis. These types of materials are being developed for potential technological applications, such as in magnetic sensors for storage devices [4].

CuFeO_2 is one of many ABO_2 type compounds where A is a nonmagnetic monovalent ion and B is a magnetic trivalent ion. These materials form a delafossite structure [5] which provide good examples of antiferromagnets on a triangular lattice [2]. It also provides the opportunity to study the influence of geometrical frustration on magnetic systems. LiCrO_2 , and CuCrO_2 are another set of materials that have the same geometrical frustration. CuFeO_2 has ABC stacking of triangular lattices of Fe^{3+} (see Fig. 1.1 (a)). Recent studies on CuFeO_2 [6, 7, 8] show that both magnetic and structural transitions occur together due to magnetoelastic coupling, at $T_{N1} \cong 14\text{K}$ and $T_{N2} \cong 11\text{K}$

at zero applied magnetic field (see Fig. 1.1).

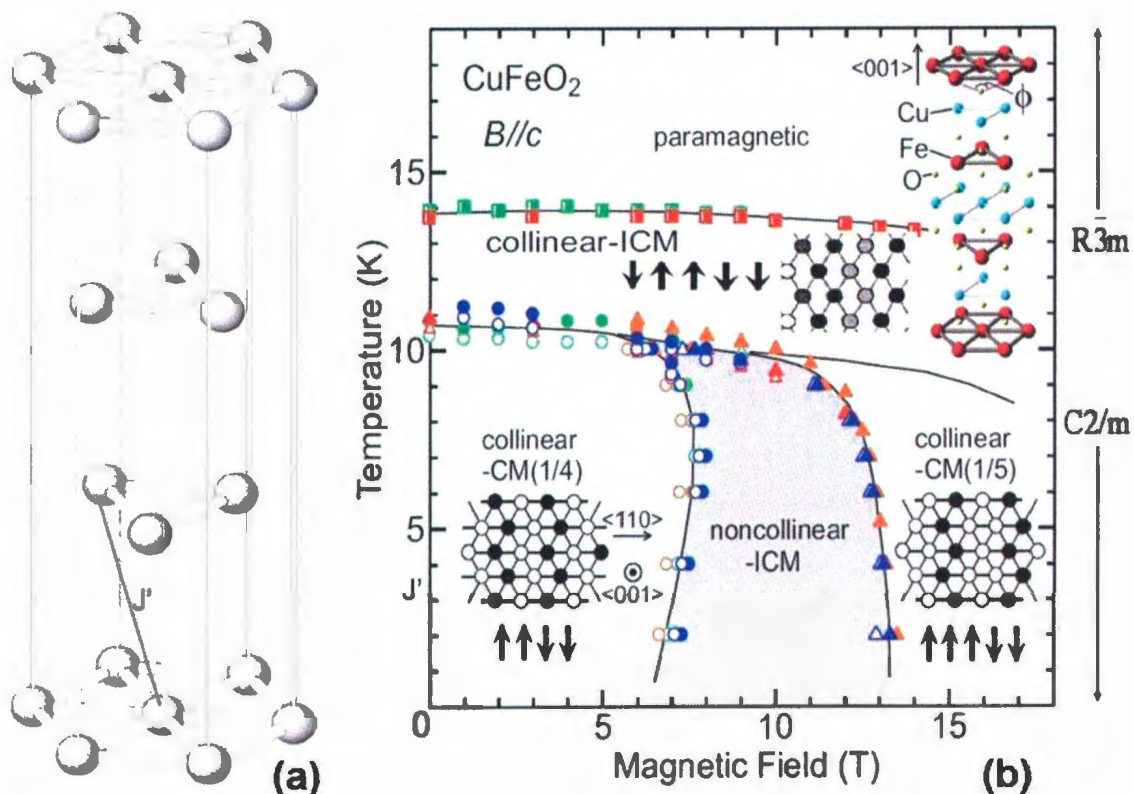


Figure 1.1: (a) Crystal structure of CuFeO_2 . Only Fe^{3+} magnetic ions are shown. (b) Temperature (T) versus magnetic field (B) phase diagram of CuFeO_2 with B applied along the c -axis [7, 8, 9].

Experimental studies [7, 8, 10] suggest CuFeO_2 undergoes many antiferromagnetic transitions (see Fig. 1.1 (b)) as a function of temperature and applied field. In zero magnetic field, successive magnetic phase transitions occur from a collinear four-sublattice phase ($\uparrow\uparrow\downarrow\downarrow$) ($T \leq T_{N2}$) with the magnetic moments along the c -axis (see Fig 1.1 (b) - CM(1/4)), through a partially incommensurate phase (see Fig. 1.1 (b)

- ICM) ($T_{N2} \leq T \leq T_{N1}$) with sinusoidally amplitude-modulated magnetic structure with magnetic moments along the c -axis. Above T_{N1} there is no long range magnetic order (paramagnetic - see Fig 1.1 (b)). Below T_{N2} , when we apply a magnetic field along the c -axis, we see that CuFeO_2 (see Fig 1.1 (b)) exhibits successive magnetic phase transitions. The inserts in Fig 1.1 show the schematic illustration of the magnetic structures on Fe^{3+} sites. With an applied magnetic field along the c -axis [7], a transition occurs from collinear four-sublattice ($\uparrow \uparrow \downarrow \downarrow$) ground state (see lower insert left area in Fig 1.1 (b)) to a field-induced incommensurate helical state at $B_1 \sim 6.5 T$ (see grey area in Fig 1.1 (b)) where spins lie in the basal plane ($\vec{s} \perp \hat{c}$), followed by a transition to a collinear commensurate five-sublattice state ($\uparrow \uparrow \uparrow \downarrow \downarrow$) at $B_2 \sim 13.5 T$ (see lower insert right area in Fig 1.1 (b)), with $\vec{s} \parallel \hat{c}$.

Let us discuss briefly the structural phase transition. A crystal is said to have a structural phase transition when its structural state (orientation state) can be shifted from one to another due to the external effect on it such as temperature, pressure, mechanical stress etc. More about it can be found in Chapter 4.

The magnetoelastic effect involves coupling between the lattice (elastic stress) and spin degrees of freedom. If this coupling is strong in a material, its elastic properties depend on its magnetic state, and its magnetic properties are influenced by the applied and internal mechanical stresses. This concept is quite general, and has been observed in ferromagnets, ferrimagnets, antiferromagnets, paramagnets, diamagnets and superconductors. Due to this magnetoelastic effect in CuFeO_2 , it has the both structural and magnetic transitions [7] at the same temperatures.

The focus of this thesis work is investigating elastic and magnetoelastic effects in CuFeO_2 , using the Landau Theory of phase transitions. This approach has been used successfully as the theoretical background of many studies of systems undergoing phase transitions. It has been demonstrated most clearly when it has been applied to intricate sequences of transitions observed in structural and magnetic systems. So first we derive relevant theories, then we analyze our problem. To discuss our results, we have

presented six chapters here. In Chapter 2, we develop the elastic theory and calculate the elastic energy and wave propagation for longitudinal and transverse ultrasonic velocities modes for CuFeO_2 . In Chapter 3, we give a short account of the Landau Theory of Phase Transitions in general. In Chapter 4, we derive our model to explain ultrasonic experimental data, which was taken here at Memorial on CuFeO_2 . Then we discuss the results of the model calculations fit to experimental data. In Chapter 5, we discuss the possible impact of the coupling between elastic and magnetic degrees of freedom. In Chapter 6, we conclude our project and discuss possible future developments.

Chapter 2

Elastic Theory

This chapter serves as a brief review of Stress and Strain in elastic media. The discussion of this chapter follows that of Dieulesaint and Royer [12], Musgrave [13] and Kittel [14]. The force acting on a unit area of an elastic body is called *Stress* and the fractional displacement is called *Strain*. Consider a simple deformation of a one dimensional example to understand these terms.

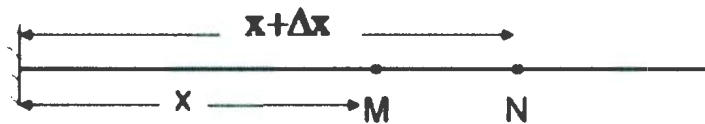


Figure 2.1: Lattice positions before the force action [12].

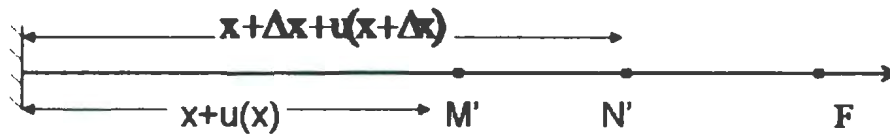


Figure 2.2: Lattice positions under the force F [12].

$$\text{Strain : } e = \lim_{\Delta x \rightarrow 0} \frac{u(x + \Delta x) - u(x)}{\Delta x} = \frac{du}{dx} \quad (2.1)$$

$$\text{Relative deformation of MN} = \frac{M'N' - MN}{MN} = \frac{u(x + \Delta x) - u(x)}{\Delta x}.$$

Next, we are going to discuss the deformations of solids. The deformations of solids depend on their shape: Under external forces, there is no reason for two points, even neighboring points to move in the same direction. Angular distortions also appear, as well as variations in length. Let us illustrate briefly.

Let O be the origin and an arbitrary point be $P(x, y, z) = \mathbf{r}$. All points in crystal move under the influence of external forces. If $\mathbf{u} = \mathbf{u}(x, y, z)$ is a continuous displacement, then the new position is

$$\mathbf{r}' = \mathbf{r} + \mathbf{u} \quad (2.2)$$

Before the force acts on it, the separation vector between two neighbouring points M and N is

$$d\mathbf{r} = \mathbf{r}_N - \mathbf{r}_M \quad (2.3)$$

Components of $d\mathbf{r}$ are dx , dy and dz , which move away from or towards each other at the same time as the orientation of MN changes. Since

$$\begin{aligned} \mathbf{r}'_M &= \mathbf{r}_M + \mathbf{u}_M, \\ \mathbf{r}'_N &= \mathbf{r}_N + \mathbf{u}_N, \\ \mathbf{u}_N &= \mathbf{u}_M + d\mathbf{u}, \text{ and} \\ d\mathbf{u} &= \frac{\partial \mathbf{u}}{\partial x} dx + \frac{\partial \mathbf{u}}{\partial y} dy + \frac{\partial \mathbf{u}}{\partial z} dz. \end{aligned}$$

Then we have

$$\begin{aligned} \mathbf{r}'_N - \mathbf{r}'_M &= \mathbf{r}_N - \mathbf{r}_M + \mathbf{u}_N - \mathbf{u}_M \\ d\mathbf{r}' &= d\mathbf{r} + d\mathbf{u} \\ (d\mathbf{r}')^2 &= (d\mathbf{r})^2 + 2 d\mathbf{r} \cdot d\mathbf{u} + (d\mathbf{u})^2 \\ (d\mathbf{r}')^2 - (d\mathbf{r})^2 &= 2 \frac{\partial u_\alpha}{\partial \beta} d\alpha d\beta + \frac{\partial u_\gamma}{\partial \alpha} \frac{\partial u_\gamma}{\partial \beta} d\alpha d\beta. \end{aligned}$$

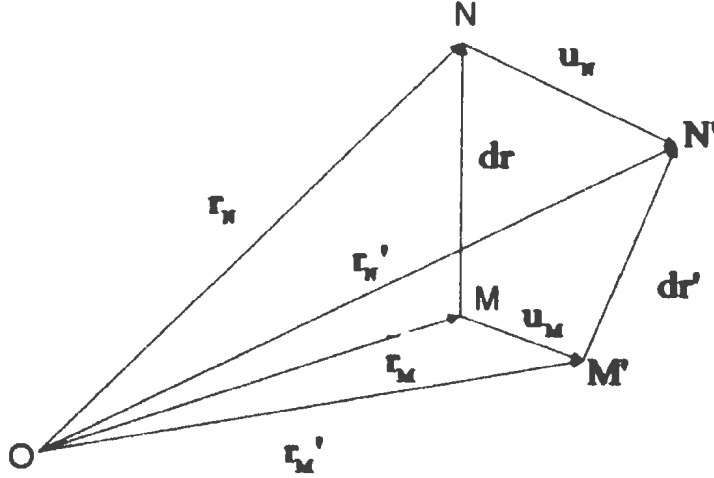


Figure 2.3: Elastic distortion [12].

where $\alpha, \beta, \gamma = x, y, z$. Permuting the dummy indices α and β , we get

$$\frac{\partial u_\alpha}{\partial \beta} d\alpha d\beta = \frac{\partial u_\beta}{\partial \alpha} d\alpha d\beta$$

$$\begin{aligned} (dr')^2 - (dr)^2 &= \left(\frac{\partial u_\alpha}{\partial \beta} + \frac{\partial u_\beta}{\partial \alpha} + \frac{\partial u_\gamma}{\partial \alpha} \frac{\partial u_\gamma}{\partial \beta} \right) d\alpha d\beta \\ &= 2e_{\alpha\beta} d\alpha d\beta \end{aligned}$$

where

$$e_{\alpha\beta} = \frac{1}{2} \left(\frac{\partial u_\alpha}{\partial \beta} + \frac{\partial u_\beta}{\partial \alpha} + \frac{\partial u_\gamma}{\partial \alpha} \frac{\partial u_\gamma}{\partial \beta} \right)$$

Since our deformations are assumed to be small, so $\frac{\partial u_\alpha}{\partial \beta} \ll 1$

This means we can ignore second order infinitesimals, so that

$$e_{\alpha\beta} = \frac{1}{2} \left(\frac{\partial u_\alpha}{\partial \beta} + \frac{\partial u_\beta}{\partial \alpha} \right) \quad (2.4)$$

Furthermore, the strain tensor is symmetric:

$$\begin{aligned} e_{\beta\alpha} &= \frac{1}{2} \left(\frac{\partial u_\beta}{\partial \alpha} + \frac{\partial u_\alpha}{\partial \beta} \right) \\ &= e_{\alpha\beta}. \end{aligned}$$

Only six components of the strain tensor $e_{\alpha\beta}$ are distinct. It depends on the point M, where the deformation is observed.

2.1 Geometrical Interpretation of strain.

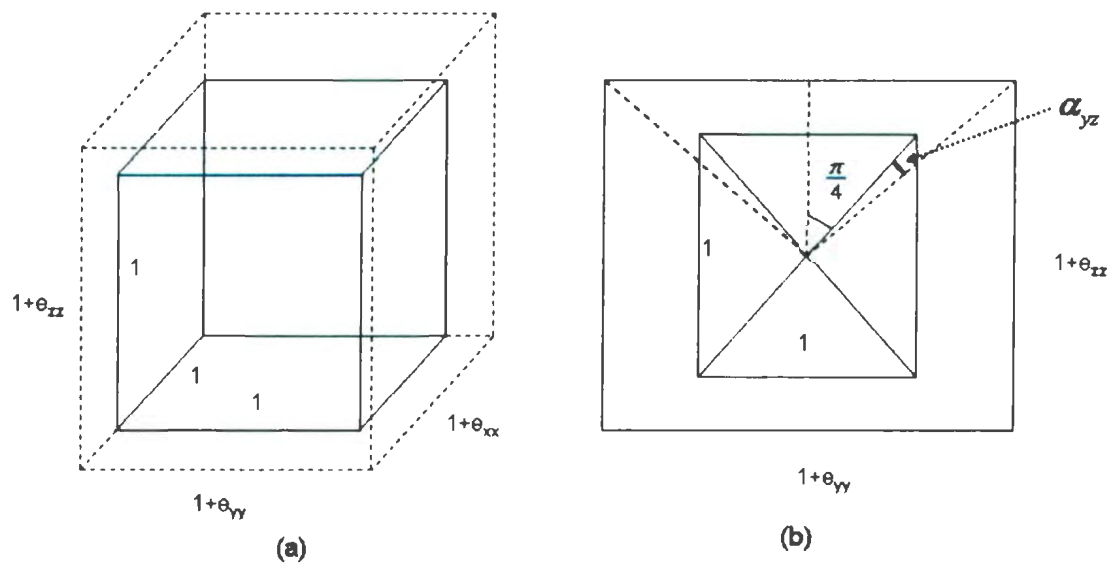


Figure 2.4: Elastic distortion: 2 D view [13].

Consider a unit cube. In Fig. 2.4 (a), the deformation of this unit cube by extensional strains e_{xx} , e_{yy} , e_{zz} parallel to the edges is shown. The volume before the deformation is $V = 1$. The volume after the deformation is given by

$$\begin{aligned} V' &= (1 + e_{xx})(1 + e_{yy})(1 + e_{zz}) \\ &= 1 + e_{xx} + e_{yy} + e_{zz} + O(e^2) \end{aligned}$$

Thus

$$\frac{\Delta V}{V} = \frac{V' - V}{V} = e_{xx} + e_{yy} + e_{zz}$$

The sum of the principal extensional strains measures dilatation, which is the fractional increase of volume associated with this deformation. This means that volume change remained invariant under rotation operations. Note that the dilations along each principal axis are given by

$$\frac{\Delta x}{x} = e_{xx}, \quad \frac{\Delta y}{y} = e_{yy}, \quad \frac{\Delta z}{z} = e_{zz}.$$

In Fig. 2.4 (b), the deformation of the face of a unit cube showing angular change α_{yz} related to the difference of principal strains e_{yy} and e_{zz} is illustrated. We have

$$\begin{aligned} \tan\left(\frac{\pi}{4} + \alpha_{yz}\right) &= \frac{1 + e_{yy}}{1 + e_{zz}} \\ \frac{1 + \tan \alpha_{yz}}{1 - \tan \alpha_{yz}} &= 1 + e_{yy} - e_{zz} + O(e^2) \end{aligned}$$

Since the deformations are small so are the α_{yz} , then we get:

$$\begin{aligned} \frac{1 + \alpha_{yz}}{1 - \alpha_{yz}} &= 1 + e_{yy} - e_{zz} \\ \alpha_{yz} &\approx e_{yy} - e_{zz} \end{aligned}$$

Similarly, we can have

$$\begin{aligned} \alpha_{zx} &\approx e_{zz} - e_{xx} \\ \alpha_{xy} &\approx e_{xx} - e_{yy} \end{aligned}$$

So

$$\alpha_{xy} + \alpha_{yz} + \alpha_{zx} = 0. \quad (2.5)$$

This means that the angular changes are not independent. We can conclude that the three principal extensional strains define one volume change and two angular or shape changes - the dilatation and two shear deformations.

2.2 Equilibrium Conditions.

In static mechanical equilibrium, the net force and torque on any given volume must be zero. Assume that stress comes from forces applied to the surface. Let $\mathbf{T}(\mathbf{r})$

be the mechanical stress on the boundary surface S at position \mathbf{r} and \mathbf{F} be the force on this volume (see Fig. 2.5). We have

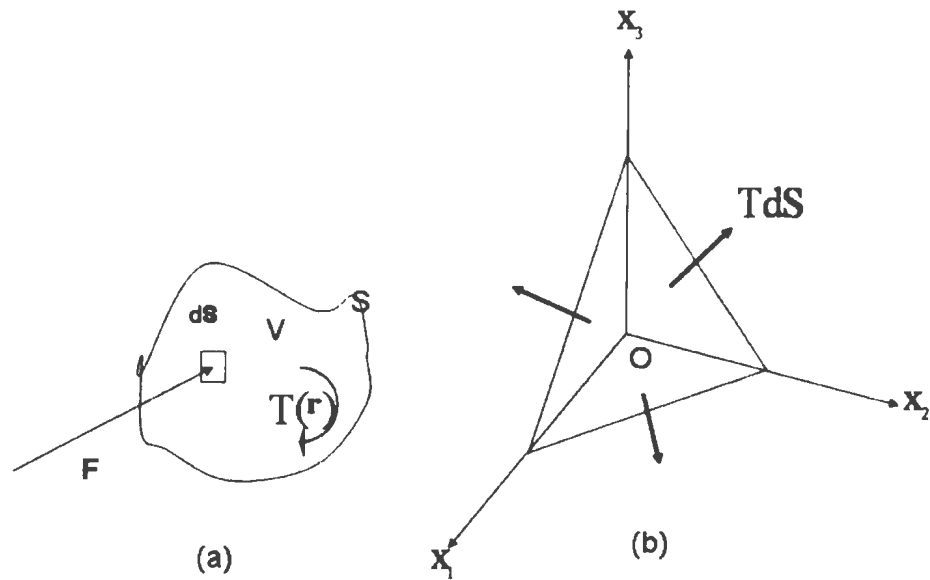


Figure 2.5: Equilibrium forces [12].

$$\begin{aligned}
 \mathbf{F} &= \int_S \mathbf{T}(\mathbf{r}) dS \\
 \mathbf{T}_i(\mathbf{r}) &= T_{ik} r_k \\
 \mathbf{F}_i &= \int_S T_{ik} r_k dS \\
 &= \int_V \frac{\partial T_{ik}}{\partial x_k} dV \quad [\text{By Green's Theorem}] \\
 f_i &= \frac{\partial T_{ik}}{\partial x_k},
 \end{aligned}$$

where f_i is density of force per unit volume of the strained medium. When the solid is subjected to forces exerted on its surface only, the static equilibrium condition is $F_i = 0 \Rightarrow f_i = 0$. Thus,

$$\frac{\partial T_{ik}}{\partial x_k} = 0 \tag{2.6}$$

Suppose we have an external force density, for example gravitational field \mathbf{g} , so the equilibrium condition becomes:

$$\frac{\partial T_{ik}}{\partial x_k} + \rho g_i = 0 \quad (2.7)$$

where ρ is the density. The torque of the stress \mathbf{T} about the origin is $\mathbf{G} = \mathbf{x} \times \mathbf{T}$. In tensor analysis, it is an antisymmetric second rank tensor $T_j x_i - T_i x_j$. The net force tensor is:

$$\begin{aligned} M_{ij} &= \int_S (T_j x_i - T_i x_j) dS \\ &= \int_S (T_{jk} x_i - T_{ik} x_j) l_k dS \\ &= \int_V \frac{\partial (T_{jk} x_i - T_{ik} x_j)}{\partial x_k} dV \quad [\text{By Green's Theorem}] \\ &= \int_V \left(\frac{\partial T_{jk}}{\partial x_k} x_i - \frac{\partial T_{ik}}{\partial x_k} x_j + T_{jk} \frac{\partial x_i}{\partial x_k} - T_{ik} \frac{\partial x_j}{\partial x_k} \right) dV \\ &= \int_V (T_{jk} \delta_{ik} - T_{ik} \delta_{jk}) dV \quad [\text{By equation (2.6)}] \end{aligned}$$

$$\text{i.e. } M_{ij} = \int_V (T_{ji} - T_{ij}) dV = 0.$$

$$T_{ji} = T_{ij}, \quad \text{for all } i \text{ and } j. \quad (2.8)$$

The stress tensor is symmetric; this reduces the number of independent components to six, which are following:

T_{11}, T_{22}, T_{33} : stress normal to the sides

T_{12}, T_{23}, T_{13} : shear stress

Suppose we have an external torque \mathbf{G} per unit volume, then the torque on the volume V is

$$M_{ij} + \int_V G_k dV,$$

where k is such that the (ijk) permutation is even. So the equilibrium conditions are:

$$T_{ji} - T_{ij} + G_k = 0 \quad (2.9)$$

We can see from the above equation that the stress tensor is no longer symmetric. This case is in practice encountered only for polar crystals in an electric field. In our

discussion, we assume that for a small torque the symmetry of the tensor T_{ij} remains unchanged.

2.3 Elastic Constants.

A medium is said to be elastic if it returns to its initial state after the external forces are removed. It returns to the initial state due to the internal stress. Let us discuss in the case of small deformations, using Taylor expansion, how we can express the stress as follows:

$$T_{ij}(e_{kl}) = T_{ij}(0) + \left(\frac{\partial T_{ij}}{\partial e_{kl}} \right)_{e_{kl}=0} e_{kl} + \frac{1}{2} \left(\frac{\partial^2 T_{ij}}{\partial e_{kl} \partial e_{mn}} \right)_{e_{kl}=0, e_{mn}=0} e_{kl} e_{mn} + \dots \quad (2.10)$$

$$\text{Since } T_{ij}(0) = 0 \quad (2.11)$$

$$T_{ij}(e_{kl}) = C_{ijkl} e_{kl} \quad [\text{Hooke's Law}] \quad (2.12)$$

$$C_{ijkl} = \left(\frac{\partial T_{ij}}{\partial e_{kl}} \right)_{e_{kl}=0} \quad (2.13)$$

The coefficient C_{ijkl} is a fourth rank tensor (the elastic stiffness tensor), T_{ij} and e_{kl} are rank two tensors.

A fourth rank tensor has $3^4 = 81$ components, but T_{ij} and e_{kl} are symmetric tensors so that

$$C_{ijkl} = C_{jikl}; \quad C_{ijkl} = C_{ijlk}. \quad (2.14)$$

Hooke's law (2.11) can be written in terms of the displacements:

$$T_{ij} = \frac{1}{2} C_{ijkl} \frac{\partial u_k}{\partial x_l} + \frac{1}{2} C_{ijkl} \frac{\partial u_l}{\partial x_k}$$

Since $C_{ijkl} = C_{ijlk}$, we have

$$T_{ij} = C_{ijkl} \frac{\partial u_l}{\partial x_k} \quad (2.15)$$

By symmetry, we are left with only 36 independent elastic constants instead of 81.

The following Voigt notation is thus useful

$$\begin{aligned} (x x) &\Leftrightarrow 1, & (y y) &\Leftrightarrow 2, & (z z) &\Leftrightarrow 3, & (y z) = (z y) &\Leftrightarrow 4, \\ (z x) = (x z) &\Leftrightarrow 5, & (x y) = (y x) &\Leftrightarrow 6 \end{aligned}$$

$$C_{\alpha\beta} = C_{ijkl}, \quad \alpha, \beta = 1, 2, 3, 4, 5, 6; \quad i, j, k, l = x, y, z.$$

$$\alpha \Leftrightarrow (ij) \quad \beta \Leftrightarrow (kl)$$

Eg: $C_{14} = C_{xxzy} = C_{xyxz}$.

Using this notation, we can rewrite equation (2.11) as follows:

$$T_{\alpha} = C_{\alpha\beta} e_{\beta} \quad (2.16)$$

$$e_1 = e_{xx}, e_2 = e_{yy}, e_3 = e_{zz}, e_4 = 2e_{yz}, e_5 = 2e_{zx}, e_6 = 2e_{xy}$$

Inversion of the Hooke's Law gives:

$$e_{ij} = S_{ijkl} T_{kl}, \quad (2.17)$$

where S_{ijkl} is called Elastic compliance constants. With the above approach, the equations become:

$$e_{\alpha} = S_{\alpha\beta} T_{\beta}$$

$$S_{\alpha\beta} = C_{\alpha\beta}^{-1}$$

$$\text{or } S_{\alpha\beta} C_{\beta\gamma} = \delta_{\alpha\gamma} \quad (2.18)$$

2.4 Elastic Energy in Distorted Media.

The energy provided by the external forces during the deformation is stored in the medium as elastic energy. After the forces are removed from it, the internal stress is released, which makes the solid return to its initial state. During the deformation, the work done by the external forces for a variation $d\mathbf{u}$ of the displacement \mathbf{u} consists of two parts: forces per unit mass \mathbf{g} and the external force \mathbf{p} acting on the surface.

$$\begin{aligned} \delta W &= \int_V \rho \mathbf{g} \cdot d\mathbf{u} \, dV + \int_S \mathbf{p} \cdot d\mathbf{u} \, dS \\ &= \int_V \rho g_i \, du_i \, dV + \int_S p_i \, du_i \, dS \end{aligned}$$

As per our assumption: The system is always in equilibrium, so this transformation is thermodynamically reversible and the equilibrium equations are valid:

$$\begin{aligned}
\delta W &= \int_V \rho g_i du_i dV + \int_S T_{ik} du_i l_k dS \\
&= \int_V \rho g_i du_i dV + \int_V \frac{\partial T_{ik}}{\partial x_k} du_i dV \\
&= \int_V \left(\rho g_i + \frac{\partial T_{ik}}{\partial x_k} \right) du_i dV + \int_V T_{ik} d \left(\frac{\partial u_i}{\partial x_k} \right) dV \\
&= \int_V T_{ik} d \left(\frac{\partial u_i}{\partial x_k} \right) dV = \int_V T_{ki} d \left(\frac{\partial u_k}{\partial x_i} \right) dV \quad [\text{By equation (2.7)}]
\end{aligned}$$

$$\begin{aligned}
\text{Thus } \delta W &= \frac{1}{2} \int_V T_{ik} d \left(\frac{\partial u_i}{\partial x_k} + \frac{\partial u_k}{\partial x_i} \right) dV \\
&= \int_V T_{ik} d S_{ik} dV \\
&= T_{ik} d S_{ik}.
\end{aligned}$$

The internal energy variation per unit volume is

$$dU = \delta W + \delta \zeta$$

where $\delta \zeta$ is the heat received per unit volume. According to the first law of thermodynamics: U is a function of state and dU is exact, while δW and $\delta \zeta$ separately are not. For a reversible transformation, the second law of thermodynamics is:

$$\delta \zeta = T d\sigma,$$

where T is the absolute temperature, σ is entropy per unit volume. So

$$\begin{aligned}
dU &= T d\sigma + T_{ik} dS_{ik} \\
U &= U(\sigma, S_{ik}) \\
\text{giving } T_{ik} &= \left(\frac{\partial U}{\partial S_{ik}} \right)_\sigma
\end{aligned}$$

Inserting similar expressions for T_{ij} and T_{kl} into (2.13), we get

$$C_{ijkl} = \frac{\partial T_{ij}}{\partial S_{kl}} \quad \text{and} \quad C_{klij} = \frac{\partial T_{kl}}{\partial S_{ij}},$$

so that,

$$C_{ijkl}^{(\sigma)} = \left(\frac{\partial^2 U}{\partial S_{ij} \partial S_{kl}} \right)_{\sigma} = C_{klij}^{(\sigma)} \quad (2.19)$$

Exchanging the first two indices with the last two does not change the value of the isentropic elastic moduli, these are involved in elastic wave propagation, where the vibration is so fast that there is no time for a thermal exchange with the external medium. Thus $\delta \zeta = 0$ implies $d\sigma = 0$.

The free energy F for isothermal transformations is given by:

$$F = U - T\sigma \quad (2.20)$$

$$dF = -\sigma dT + T_{ik} dS_{ik} \quad (2.21)$$

$$F = F(T, S_{ik}) \quad (2.22)$$

So that $T_{ik} = \left(\frac{\partial F}{\partial S_{ik}} \right)_T$ and for isothermal elastic constants:

$$C_{ijkl}^{(T)} = \left(\frac{\partial^2 F}{\partial S_{ij} \partial S_{kl}} \right)_T = C_{klij}^{(T)} \quad (2.23)$$

Within the domain of validity of Hooke's Law,

$$dU = Td\sigma + C_{ijkl}^{(\sigma)} S_{kl} dS_{ij}.$$

After permuting the dummy indices (ij) and (kl) , we get

$$\begin{aligned} dU &= Td\sigma + \frac{1}{2}(C_{ijkl}^{(\sigma)} S_{kl} dS_{ij} + C_{klij}^{(T)} S_{ij} dS_{kl}) \\ &= Td\sigma + \frac{1}{2}C_{ijkl}^{(\sigma)} d(S_{ij} S_{kl}) \end{aligned}$$

Integrating this relation gives

$$U(\sigma, s_{ik}) = U_o(\sigma) + \frac{1}{2}C_{ijkl}^{(\sigma)} S_{ij} S_{kl},$$

where $U_o(\sigma)$ is the internal energy of the undeformed medium: $U_o(\sigma) = U_o(\sigma, S_{ik} = 0)$.

In a similar way, we can have the expression for free energy:

$$F(T, s_{ik}) = F_o(T) + \frac{1}{2}C_{ijkl}^{(T)} S_{ij} S_{kl}.$$

Thus the elastic potential energy Φ is

$$\Phi = \frac{1}{2} C_{ijkl}^{(T)} S_{ij} S_{kl}.$$

With the elastic moduli in matrix notation expressed as

$$\begin{pmatrix} C_{11} & C_{12} & C_{13} & C_{14} & C_{15} & C_{16} \\ C_{12} & C_{22} & C_{23} & C_{24} & C_{25} & C_{26} \\ C_{13} & C_{23} & C_{33} & C_{34} & C_{35} & C_{36} \\ C_{14} & C_{24} & C_{34} & C_{44} & C_{45} & C_{46} \\ C_{15} & C_{25} & C_{35} & C_{45} & C_{55} & C_{56} \\ C_{16} & C_{26} & C_{36} & C_{46} & C_{56} & C_{66} \end{pmatrix} \quad (2.24)$$

The most general crystal system with only translational symmetry is triclinic. In this case all 21 components of the elastic tensor are independent. For other crystal systems with point groups symmetries, we can reduce the number of independent components. The physical constants of an isotropic medium do not depend on the choice of the orthonormal reference frame. Elasticity tensor C_{ijkl} must be invariant under all transformations of the reference frame (rotation, symmetry with respect to a point or a plane etc..).

2.5 Crystals

The general invariance condition for a stiffness tensor is:

$$c_{ijkl} = \alpha_i^p \alpha_j^q \alpha_k^r \alpha_l^s c_{pqrs} \quad (2.25)$$

where α represent the point groups element operation for a given crystal symmetry and α_i^p represents the i th element of α . We can derive any crystal's independent elastic stiffness constants by using point group symmetry operations. Note that it is enough to use the generators of the Point group element class to find the symmetry of the elastic tensor a given crystal class.

Example: For trigonal system:

Generators for this crystal are I (inversion) and C_3^+ (three fold rotation), which is

$$C_3^+ = \begin{pmatrix} -\frac{1}{2} & \frac{\sqrt{3}}{2} & 0 \\ -\frac{\sqrt{3}}{2} & -\frac{1}{2} & 0 \\ 0 & 0 & 1 \end{pmatrix} \quad (2.26)$$

First we apply the rotation (2.26) to elastic stiffness tensor matrix (2.24), we get

$$(C_{\alpha\beta}) = \begin{pmatrix} C_{11} & C_{12} & C_{13} & C_{14} & -C_{15} & 0 \\ C_{12} & C_{11} & C_{13} & -C_{14} & C_{15} & 0 \\ C_{13} & C_{13} & C_{33} & 0 & 0 & 0 \\ C_{14} & -C_{14} & 0 & C_{44} & 0 & C_{15} \\ -C_{15} & C_{15} & 0 & 0 & C_{44} & C_{14} \\ 0 & 0 & 0 & C_{15} & C_{14} & \frac{C_{11}-C_{12}}{2} \end{pmatrix} \quad (2.27)$$

For any one of the point groups element classes $\bar{3}m$, 32 or $3m$, the elastic stiffness tensor matrix (2.27) then reduces to

$$(C_{\alpha\beta}) = \begin{pmatrix} C_{11} & C_{12} & C_{13} & C_{14} & 0 & 0 \\ C_{12} & C_{11} & C_{13} & -C_{14} & 0 & 0 \\ C_{13} & C_{13} & C_{33} & 0 & 0 & 0 \\ C_{14} & -C_{14} & 0 & C_{44} & 0 & 0 \\ 0 & 0 & 0 & 0 & C_{44} & C_{14} \\ 0 & 0 & 0 & 0 & C_{14} & \frac{C_{11}-C_{12}}{2} \end{pmatrix} \quad (2.28)$$

2.6 Elastic Energy

The elastic energy of a crystal system is a quadratic function of the strains, in the approximation of the Hooke's law (similar to the expression for the energy of a stretched spring). Thus we may write

$$F_e(e) = \frac{1}{2} \sum_{i,j} e_i C_{ij} e_j, \quad (2.29)$$

where C_{ij} is elastic stiffness tensor and e_i is strain tensor. Therefore, the elastic energy expression (2.29) becomes for high temperature $R\bar{3}m$ phase of CuFeO_2 ,

$$F_e(e) = \frac{1}{2}C_p(e_1 + e_2)^2 + \frac{1}{2}C_{33}e_3^2 + \frac{1}{2}C_{44}(e_4^2 + e_5^2) + \frac{1}{2}C_{66}e_6^2 + \frac{1}{2}C_{66}(e_1 - e_2)^2 + C_{13}(e_1 + e_2)e_3 + C_{14}(e_1e_4 - e_2e_4 + e_5e_6) \quad (2.30)$$

where $C_p = \frac{C_{11}+C_{12}}{2}$ and $C_{66} = \frac{C_{11}-C_{12}}{2}$.

2.7 Elastic Waves

2.7.1 Brief Note about waves

There are a great variety of elastic waves. Some examples are Rayleigh waves, Bleustein - Gulyaev waves, Lamb Waves, Love waves and Stonely waves. There are two common types of waves: (1) *Longitudinal waves or Compression waves*: Particle displacement is parallel to the direction of the propagation. Polarization is parallel to the wave vector. (2) *Transverse waves or Shear waves*: Particle displacement is perpendicular to the direction of the propagation. (In the most general case, none of the wave is purely longitudinal or transverse.) For any given direction, there can be three waves:

- A quasi longitudinal wave (particle vibration and the wave vector make a non-vanishing angle)
- A fast quasi-transverse wave
- A slow quasi-transverse wave

The polarizations of these three waves (with different propagation velocities) are always mutually orthogonal.

2.7.2 Elastic Waves in an Infinite Crystal:

The displacement of any point in a crystal depends on the initial coordinates x_k and time t , and is

$$u_i = U_i(x_k, t), \quad (2.31)$$

where x_k is the initial coordinates. Let us derive the propagation equation for a wave in the crystal.

Propagation Equation:

The force density per unit volume of stressed material is given by

$$f_i = \frac{\partial T_{ij}}{\partial x_j}$$

We neglect effects due to gravity and all other external forces. So the acceleration $\frac{\partial^2 u_i}{\partial t^2}$ along the i^{th} axis for the unit volume mass ρ obeys

$$\rho \frac{\partial^2 u_i}{\partial t^2} = \frac{\partial T_{ij}}{\partial x_j}.$$

By using Hooke's Law:

$$T_{ij} = C_{ijkl} \frac{\partial u_l}{\partial x_k},$$

the equations of motion become

$$\rho \frac{\partial^2 u_i}{\partial t^2} = C_{ijkl} \frac{\partial^2 u_l}{\partial x_l \partial x_k} \quad (2.32)$$

This is a set of three second order differential equations for wave propagation.

The propagation equation in a fluid is isotropic so that

$$\rho \frac{\partial^2 u}{\partial t^2} = \frac{1}{\chi} \frac{\partial^2 u}{\partial x^2}$$

The general solution for it is given by

$$u = F\left(t - \frac{x}{v}\right) \quad \text{with} \quad v^2 = \frac{1}{\rho\chi}$$

So by using this analogy, solution for equation (2.32) is a wave, traveling in the direction of the unit vector $\mathbf{n}(n_1, n_2, n_3)$ perpendicular to the wave planes $\mathbf{n} \cdot \mathbf{x} = \varepsilon_{te}$:

$$u_i = u_i F\left(t - \frac{\mathbf{n} \cdot \mathbf{x}}{v}\right) = u_i F\left(t - \frac{n_j \cdot x_j}{v}\right) \quad (2.33)$$

To calculate the phase velocity v and the wave polarization u (i.e. particle displacement) using equations (2.32) and (2.33), we get

$$\begin{aligned} \frac{\partial u_i}{\partial x_j} &= -u_i F' \frac{n_j}{v} \\ \frac{\partial^2 u_i}{\partial x_j \partial x_k} &= u_i F'' \frac{n_j n_k}{v^2} \\ \text{So } \rho u_i F'' &= C_{ijkl} n_j n_k n_l \frac{F''}{v^2} \\ \text{or } \rho v^2 u_i &= C_{ijkl} n_j n_k n_l, \end{aligned}$$

where

$$\Gamma_{il} = C_{ijkl} n_j n_k \quad (2.34)$$

and the Christoffel equation is

$$\Gamma_{il} u_l = \rho v^2 u_i, \quad (2.35)$$

where u_i is an eigenvector of the Γ_{il} tensor with eigenvalue $\rho v^2 = \gamma$. Finally, the velocities and polarizations of those plane waves with a stiffness tensor C_{ijkl} are obtained by solving for the eigenvalues and eigenvectors of the tensor $\Gamma_{il} = C_{ijkl} n_j n_k$. Generally, for a given propagation direction, there are three velocities, which means that there are three roots of the following *secular equation*:

$$|\Gamma_{il} - \rho v^2 \delta_{il}| = 0 \quad (2.36)$$

Properties of Elastic Plane Waves:

Note that $\Gamma_{li} = C_{ljki} n_j n_k = C_{klij} n_j n_k = C_{ijkl} n_j n_k = \Gamma_{il}$, which means that $\Gamma_{li} = \Gamma_{il}$

The eigenvalues of Γ_{il} are *real* and they are positive. Since the eigenvalues are real and positive, there are in general three waves propagating in the same direction with

different velocities, and mutually orthogonal polarizations.

Example: Trigonal System:

Recall the elastic Stiffness tensor matrix (2.28):

$$(C_{\alpha\beta}) = \begin{pmatrix} C_{11} & C_{12} & C_{13} & C_{14} & 0 & 0 \\ C_{12} & C_{11} & C_{13} & -C_{14} & 0 & 0 \\ C_{13} & C_{13} & C_{33} & 0 & 0 & 0 \\ C_{14} & -C_{14} & 0 & C_{44} & 0 & 0 \\ 0 & 0 & 0 & 0 & C_{44} & C_{14} \\ 0 & 0 & 0 & 0 & C_{14} & \frac{C_{11}-C_{12}}{2} \end{pmatrix} \quad (2.37)$$

The propagation tensor components are

$$\begin{aligned} \Gamma_{11} &= C_{11} n_1^2 + C_{66} n_2^2 C_{44} n_3^2 + 2 C_{14} n_2 n_3 \\ \Gamma_{12} &= (C_{12} + C_{66}) n_1 n_2 + 2 C_{14} n_1 n_3 \\ \Gamma_{13} &= 2 C_{14} n_1 n_2 + (C_{13} + C_{44}) n_1 n_3 \\ \Gamma_{22} &= C_{66} n_1^2 + C_{11} n_2^2 + C_{44} n_3^2 - 2 C_{14} n_2 n_3 \quad \text{with } C_{66} = \frac{C_{11} - C_{12}}{2} \\ \Gamma_{23} &= C_{14} (n_1^2 - n_2^2) + (C_{13} + C_{44}) n_2 n_3 \\ \Gamma_{33} &= C_{44} (n_1^2 + n_2^2) + C_{33} n_3^2 \end{aligned} \quad (2.38)$$

For example if propagation is along the x axis, $n_1 = 1$, $n_2 = 0$, $n_3 = 0$, and our tensor Γ_{ij} is

$$\Gamma = \begin{pmatrix} C_{11} & 0 & 0 \\ 0 & C_{66} & C_{14} \\ 0 & C_{14} & C_{44} \end{pmatrix}$$

which implies a longitudinal wave of velocity $V = \sqrt{\frac{C_{11}}{\rho}}$, its polarization is $(1, 0, 0)$ and two shear waves of velocities V_2 and V_3 such that

$$2\rho V_2^2 = C_{44} + C_{66} + \sqrt{(C_{44} - C_{66})^2 + 4C_{14}^2} \quad (2.39)$$

$$2\rho V_3^2 = C_{44} + C_{66} - \sqrt{(C_{44} - C_{66})^2 + 4C_{14}^2} \quad (2.40)$$

and its polarizations are $\left(0, -\frac{C_{44} - C_{66} + \sqrt{(C_{44} - C_{66})^2 + 4C_{14}^2}}{2C_{14}}, 1\right)$ and

$\left(0, -\frac{C_{44} - C_{66} - \sqrt{(C_{44} - C_{66})^2 + 4C_{14}^2}}{2C_{14}}, 1\right)$ respectively for each shear waves.

In a similar way, we can calculate other propagations along the y and z axes. We list these in the following Table 2.1 for Trigonal crystals. Table 2.2 contains the expression for ρv^2 and propagation for Monoclinic crystals.

In next chapter, we review the Landau theory of phase transitions.

Table 2.1: Polarizations and expressions ρv^2 for velocities for Trigonal ($R\bar{3}m$) Crystals

Direction of propagation	Polarization	Velocity
[100]	[100] L $\left(0, -\frac{C_{44} - C_{66} + \sqrt{(C_{44} - C_{66})^2 + 4C_{14}^2}}{2C_{14}}, 1\right)$	C_{11} $\frac{1}{2}(C_{44} + C_{66} - \sqrt{(C_{44} - C_{66})^2 + 4C_{14}^2})$
	$\left(0, -\frac{C_{44} - C_{66} - \sqrt{(C_{44} - C_{66})^2 + 4C_{14}^2}}{2C_{14}}, 1\right)$	$\frac{1}{2}(C_{44} + C_{66} + \sqrt{(C_{44} - C_{66})^2 + 4C_{14}^2})$
[010]	[100] T $\left(0, -\frac{C_{11} - C_{44} - \sqrt{(C_{11} - C_{44})^2 + 4C_{14}^2}}{2C_{14}}, 1\right)$	C_{66} $\frac{1}{2}(C_{11} + C_{44} - \sqrt{(C_{11} - C_{44})^2 + 4C_{14}^2})$
	$\left(0, -\frac{C_{11} - C_{44} + \sqrt{(C_{11} - C_{44})^2 + 4C_{14}^2}}{2C_{14}}, 1\right)$	$\frac{1}{2}(C_{11} + C_{44} + \sqrt{(C_{11} - C_{44})^2 + 4C_{14}^2})$
[001]	[001] L [010] T [100] T	C_{33} C_{44} C_{44}

Table 2.2: Polarizations and expressions ρv^2 for velocities for Monoclinic (2/m) Crystals. Note that we are using a coordinate system with the twofold symmetry axis parallel to \hat{x} , not the conventional setting of twofold symmetry axis parallel to \hat{z} .

Direction of propagation	Polarization	Velocity
[100]	[100] L $\left(0, -\frac{C_{55} - C_{66} - \sqrt{(C_{55} - C_{66})^2 + 4C_{56}^2}}{2C_{56}}, 1 \right)$	C_{11} $\frac{1}{2}(C_{55} + C_{66} + \sqrt{(C_{55} - C_{66})^2 + 4C_{56}^2})$
	$\left(0, -\frac{C_{55} - C_{66} + \sqrt{(C_{55} - C_{66})^2 + 4C_{56}^2}}{2C_{56}}, 1 \right)$	$\frac{1}{2}(C_{55} + C_{66} - \sqrt{(C_{55} - C_{66})^2 + 4C_{56}^2})$
[010]	[100] T $\left(0, -\frac{-C_{22} + C_{44} + \sqrt{(C_{22} - C_{44})^2 + 4C_{24}^2}}{2C_{24}}, 1 \right)$	C_{66} $\frac{1}{2}(C_{22} + C_{44} - \sqrt{(C_{22} - C_{44})^2 + 4C_{24}^2})$
	$\left(0, -\frac{-C_{22} + C_{44} - \sqrt{(C_{22} - C_{44})^2 + 4C_{24}^2}}{2C_{24}}, 1 \right)$	$\frac{1}{2}(C_{22} + C_{44} + \sqrt{(C_{22} - C_{44})^2 + 4C_{24}^2})$
[001]	$\left(0, -\frac{C_{33} - C_{44} - \sqrt{(C_{33} - C_{44})^2 + 4C_{34}^2}}{2C_{34}}, 1 \right)$	$\frac{1}{2}(C_{33} + C_{44} + \sqrt{(C_{33} - C_{44})^2 + 4C_{34}^2})$
	[100] T $\left(0, -\frac{C_{33} - C_{44} + \sqrt{(C_{33} - C_{44})^2 + 4C_{34}^2}}{2C_{34}}, 1 \right)$	C_{55} $\frac{1}{2}(C_{33} + C_{44} - \sqrt{(C_{33} - C_{44})^2 + 4C_{34}^2})$

Chapter 3

Landau Theory of Phase Transitions.

3.1 Brief Introduction

A phase characterizes a given assembly of atoms or molecules, which can be described by thermodynamic variables such as volume V , pressure P , temperature T and the free energy F . A phase transition or phase change is the transformation of a thermodynamic system from one phase to another. The distinguishing characteristic of a phase transition is an abrupt sudden change in one or more physical quantities (e.g. heat capacity, volume, entropy, etc...). The identification of this property (these properties are) an important step to understand this considered transition. Let us describe this transition by using the free energy F . When the free energy is a minimum, the phase will be stable under some specified thermodynamic conditions. As the thermodynamic variables such as temperature, pressure, volume or any other variables acting on the system is changed, the free energy is also changed. Whenever we have such variations in free energy, we can have changes which lead to the free energy being minimized by a different phase of our system. By minimizing the free energy we can thus describe phase transitions.

Landau theory is useful to understand structural phase transitions. The procedure of this theory is general and is one of the most useful tools in condensed matter physics. By using it, we can describe and understand the nature of phase transitions among the states both ordered (low temperature phase) and disordered (high temperature phase). We can also use it as a starting point for understanding the behavior of ordered states. The discussion in this chapter follows that of Tolédano [15], Salje [16] and Burns [17].

A phase transition is characterized by an *order parameter* (Q), which can characterize an atomic displacement, electric polarization, magnetization etc. It is non zero at low temperature and becomes zero above a certain temperature T_c , which is called the transition temperature. Transitions are said to be *continuous/ second order phase transitions* if its order parameter decreases continuously to zero as the high-symmetry phase is approached (see Fig. 3.1 (b)) and discontinuous transitions are said to be *first order phase transitions*, and in that case the magnitude of the order parameter changes suddenly at T_c as illustrated in Fig. 3.1 (a). Note that since we will be concerned only with uniform deformations, gradient terms in the free energy are zero. Let us begin with a discussion of symmetry.

3.2 Role of Symmetry.

Let us now talk briefly about how the space group/subgroup play a role in phase transitions and Landau theory. For some transitions, the physical quantity which characterizes the transition not only changes between the two phases, but it is also changes in each phase when some external variables such as temperature or pressure are modified. For example the case of the liquid-vapour transition, a relevant property is the fluid's density (or specific volume). We need to give qualitative differences between phases, which can be defined precisely in terms of symmetry. The symmetry of a phase is characterized by its space group, which contains the set of geometrical transformations. The geometrical transformations are all possible transformations such

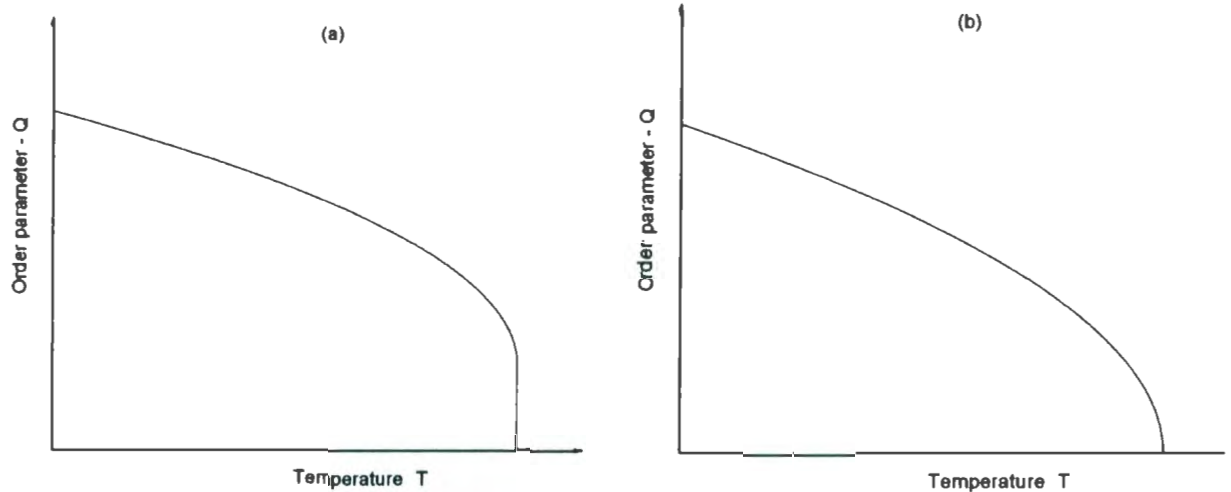


Figure 3.1: Order parameter as a function of temperature. Plot (a) represents a first order transition, here Q decreases to zero discontinuously at T_c . Plot (b) represents a second order transition, Q decreases to zero continuously at T_c [15].

as rotations, reflection, inversion etc such that the system remains unchanged. So phase transitions can be described in another way, as a symmetry change from one phase to another phase [18].

Phase transitions also satisfy a group/subgroup relation: In a phase transition, if phase I represents a (space) group G_o and phase II represents another (space) group G , then G is a subgroup of G_o . To illustrate this, let us consider our thesis project phase transition in CuFeO_2 : $\text{R}\bar{3}\text{m} \rightarrow \text{C}2/\text{m}$. Consider the unit cell of the crystal CuFeO_2 (see Fig. 3.2). Phase I (trigonal) is left invariant by symmetry elements of $\text{R}\bar{3}\text{m}$ (symmetry elements of $\text{R}\bar{3}\text{m}$ are $E, C_3^+, C_3^-, C_{2x}, C_{2y}, C_{2z}, I, S_6^+, S_6^-, \sigma_{xy}, \sigma_{yz}, \sigma_{zx}$). Clearly the product any two symmetries will also leave the structure unchanged. The phase II (monoclinic) (see Fig. 3.2 (b)) is left invariant by its space group $\text{C}2/\text{m}$ (symmetry elements of $\text{C}2/\text{m}$ are E, C_{2z}, I, σ_z). We can see from this that elements of $\text{C}2/\text{m}$ also belong to $\text{R}\bar{3}\text{m}$: $\text{C}2/\text{m}$ is a subgroup of $\text{R}\bar{3}\text{m}$.

In Landau theory, the free energy must be invariant with respect to space group symmetry and the Landau free energy can be expanded as a power series of order

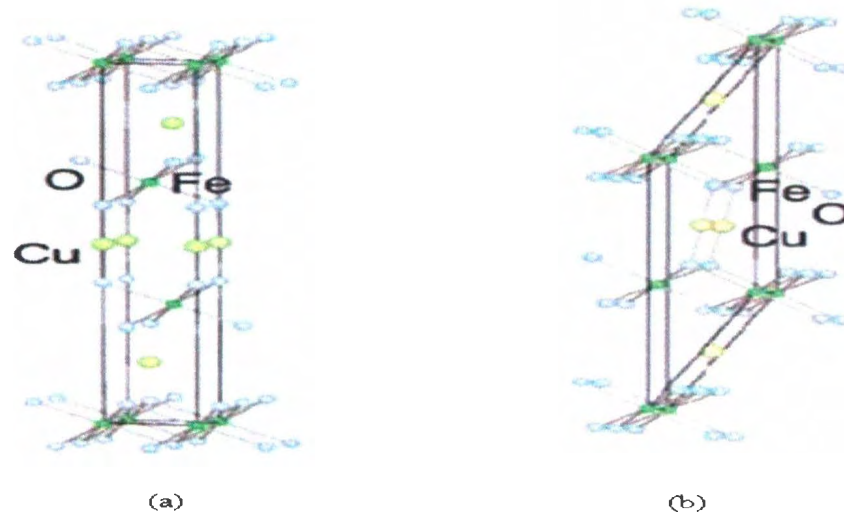


Figure 3.2: (a) Represents the $R\bar{3}m$ space group structure (Trigonal), (b) represents $C2/m$ space group structure (Monoclinic) [19].

parameters near the transition temperature. Space group symmetries determine the systems properties and the possible phase transitions that can occur.

3.3 Landau free energy for the simplest case of one order parameter: Even order invariants of the order parameter

In the vicinity of a phase transition one can expand the Landau free energy in a power series of order parameter. Let us begin with following general form up to sixth order:

$$F_L(Q) = A_0 + A_1 Q + \frac{1}{2} A Q^2 + \frac{1}{3} b Q^3 + \frac{1}{4} B Q^4 + \frac{1}{5} c Q^5 + \frac{1}{6} C Q^6. \quad (3.1)$$

The first derivative of $F_L(Q)$ is:

$$\frac{\partial F_L(Q)}{\partial Q} = A_1 + A Q + b Q^2 + B Q^3 + c Q^4 + C Q^5. \quad (3.2)$$

At high temperatures, the order parameter Q is always zero. Then equation (3.2) becomes

$$\frac{\partial F_L(Q)}{\partial Q} = A_1.$$

For the minimum of $F_L(Q)$ (since any stable state corresponds to a minimum of F_L), the first derivative of $F_L(Q)$ must be zero. Hence $A_1 = 0$. $F_L - A_0$ represents the change in Landau free energy, so it is convenient to set $A_0 = 0$.

$F_L(Q)$ is constructed so as to be invariant with respect to the symmetry of the high temperature phase I. So symmetry of the system plays an important role to determine the Landau free energy for a given system. Suppose we have any symmetry which gives $Q \rightarrow -Q$, then the system can have only even powers of Q . Let us assume in this section of our discussion we have this inversion symmetry. So (3.1) becomes

$$F_L(Q) = \frac{1}{2} A Q^2 + \frac{1}{4} B Q^4 + \frac{1}{6} C Q^6. \quad (3.3)$$

where A is assumed to be strongly temperature dependent, and both B (which can be either $B > 0$ or $B < 0$) and C (always $C > 0$) are assumed to be constant for $T \sim T_c$.

Let us now look at this power series to see under what conditions there is a minimum which moves around as we change the temperature. First, we assume A , B and C are all positive. Then all of the terms increase the Landau free energy for all values of Q , so the minimum occurs when $Q = 0$. This describes the disordered phase. In the ordered phase, one of them must be negative and this constant to be large enough compared to the others. As A is temperature dependent in the Landau's assumption, we can take $A = a(T - T_0)$, with $a > 0$, where T_0 is transition temperature. Then the Landau free energy (3.3) becomes

$$F_L(Q) = \frac{1}{2} a(T - T_0) Q^2 + \frac{1}{4} B Q^4 + \frac{1}{6} C Q^6. \quad (3.4)$$

To analyze further, we can have two main situations based on the sign of constant B :

- $B > 0$ - Second Order Phase Transitions (Continuous Transitions)
- $B < 0$ - First Order Phase Transitions (Discontinuous Transitions)

3.3.1 Second Order Transitions: 2-4 potential

The transition is second order if $B > 0$. In this case, let us consider the simplest case of F_L (2-4 potential): We neglect the sixth power term from our calculation. So equation (3.4) becomes:

$$F_L(Q) = \frac{1}{2} a(T - T_o) Q^2 + \frac{1}{4} B Q^4. \quad (3.5)$$

The equations minimizing $F_L(Q)$ are:

$$\frac{\partial F_L(Q)}{\partial Q} = Q(a(T - T_o) + BQ^2) = 0 \quad (3.6)$$

$$\frac{\partial^2 F_L(Q)}{\partial Q^2} = a(T - T_o) + 3BQ^2 \geq 0 \quad (3.7)$$

Solution of (3.6) is

$$\begin{aligned} Q &= \sqrt{\frac{a(T_o - T)}{B}}, & T < T_o \\ Q &= 0, & T > T_o \end{aligned} \quad (3.8)$$

The first solution represent the low temperature phase ($T < T_o$) and the second corresponds that high temperature phase ($T > T_o$), where $T_c = T_o$ is the critical temperature (transition temperature). (see Fig. 3.3).

3.3.2 First Order Transitions: 2-4-6 potential

The transition is first order if $B < 0$. In this case, we need to keep sixth power term in our calculation to restrain $F_L(Q)$ (2-4-6 potential) from going to minus infinity (see Fig. 3.4(a)).

The equations minimizing $F_L(Q)$ are:

$$\frac{\partial F_L(Q)}{\partial Q} = Q(a(T - T_o) + BQ^2 + CQ^4) = 0 \quad (3.9)$$

$$\frac{\partial^2 F_L(Q)}{\partial Q^2} = a(T - T_o) + 3BQ^2 + 5CQ^4 \geq 0 \quad (3.10)$$

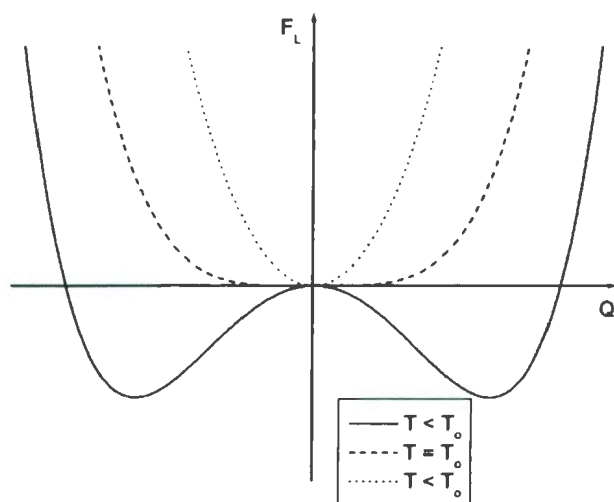


Figure 3.3: Free energy F_L is a function of the order parameter Q for various values of temperature T . The minima occur at the equilibrium values of Q for each T [15].

For $T > T_2 = T_0 + \frac{B^2}{4aC}$ only one real root of (3.9) is $Q = 0$, because of $B^2 - 4aC(T - T_0) < 0$, so we can have only one stable phase, namely the parent phase I.

At $T = T_2$ phase II with

$$Q = \pm \left(\frac{-B + \sqrt{B^2 - 4aC(T - T_0)}}{2C} \right)^{\frac{1}{2}}. \quad (3.11)$$

appears as a metastable state (i.e. it is corresponding to secondary minima in the non-equilibrium curve $F_L(Q)$ [Fig. 3.4(a)]).

For $T < T_2$, the stability of phase II increases. Phase I and II are equally stable at $T = T_1$, where T_1 is found, when the additional condition $F_L(Q) = 0$ is fulfilled, i.e.

$$F_L(Q) = 0 \Rightarrow \frac{1}{2} a(T - T_0) Q^2 + \frac{1}{4} B Q^4 + \frac{1}{6} C Q^6 = 0$$

$$Q = 0 \quad , \quad Q = \pm \left(\frac{-3B + \sqrt{9B^2 - 48aC(T - T_0)}}{4C} \right)^{\frac{1}{2}}$$

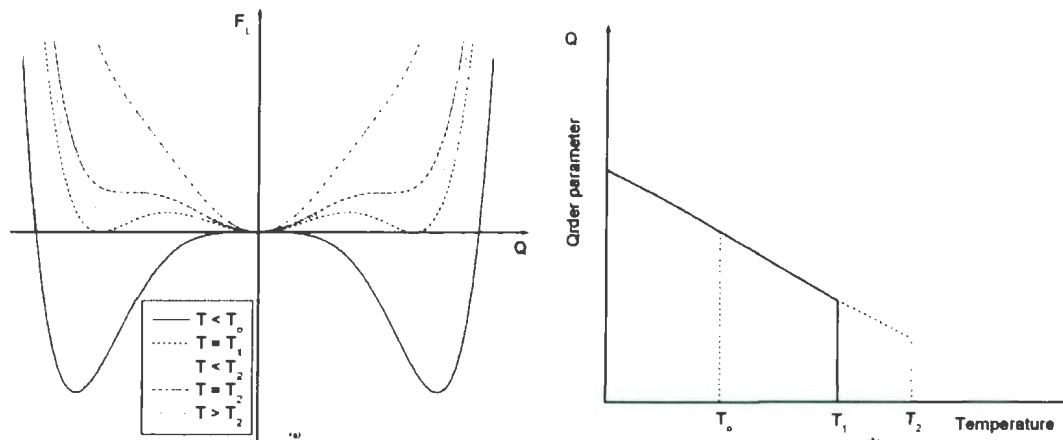


Figure 3.4: (a) Variation of the non-equilibrium potential F_L as a function of temperature, (b) Temperature dependence of the order parameter [15].

For a real solution: $9B^2 - 48aC(T - T_0) \geq 0$, which leads,

$$T \leq T_1 = T_0 + \frac{3B^2}{16aC}. \quad (3.12)$$

Below T_1 , phase I becomes less stable than Phase II, and remains as a metastable state until B changes sign for $T = T_0$. Thus, a first order phase transition occurs at $T = T_1$.

3.4 2-3-4 Potential: Landau free energy for simplest case of one order parameter.

We now consider cases where a third order (Q^3) contribution to $F_L(Q)$ is allowed by symmetry. The Landau free energy expression for this case is, (with $C \equiv 0$ for convenience).

$$F_L(Q) = \frac{1}{2}a(T - T_0)Q^2 + \frac{1}{3}bQ^3 + \frac{1}{4}BQ^4. \quad (3.13)$$

The minima equations are

$$\frac{\partial F_L(Q)}{\partial Q} = Q(a(T - T_0) + bQ + BQ^2) = 0 \quad (3.14)$$

$$\frac{\partial^2 F_L(Q)}{\partial Q^2} = a(T - T_o) + 2bQ + 3BQ^2 \geq 0 \quad (3.15)$$

Assuming $b < 0$, $B > 0$, as we discussed in the above, we can have

$$T_1 = T_o + \frac{2b^2}{9aB}, \quad (3.16)$$

the low-temperature phase appears as metastable. The high and low temperature phases are equally stable for:

$$T_2 = T_o + \frac{b^2}{4aB}, \quad (3.17)$$

The transition is always first order if a third order (Q^3) term is allowed by symmetry in the free energy. The Fig. 3.5 illustrates the transition.

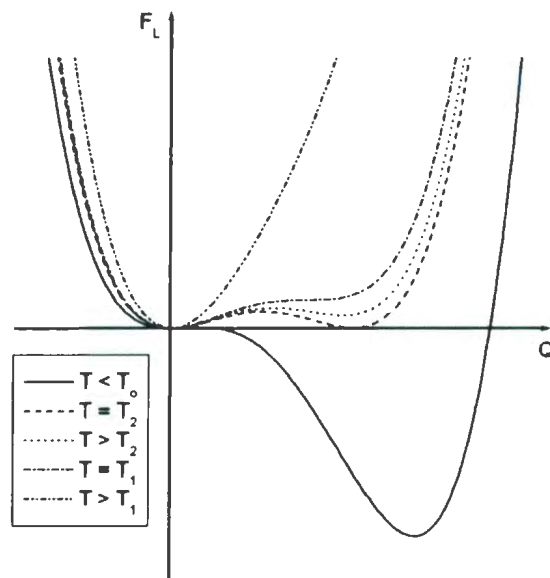


Figure 3.5: Variation of the non-equilibrium potential F_L as a function of temperature [15].

Based on the basic principles of the Landau theory of phase transition described in this chapter, we can now apply this to the structural phase transition in CuFeO_2 .

Chapter 4

Landau Free Energy Analysis of Ultrasonic Data on the Ferroelastic $R\bar{3}m \rightarrow C2/m$ Transition in CuFeO_2 .

4.1 Brief Introduction

In this chapter, we are going to use Landau theory to investigate the $R\bar{3}m \rightarrow C2/m$ structural phase transition in CuFeO_2 . First, we derive a Landau free energy compatible with the symmetry properties associated with the $R\bar{3}m$ high temperature phase. Then, we verify the compatibility of our theoretical results with experimental observations obtained on CuFeO_2 . In particular, we compare theoretical calculations with elastic constants determined from ultrasonic sound velocity measurements, realized as a function of temperature by Dr. Guy Quirion at Memorial University.

As shown in Fig. 4.1, the data on the elastic constant C_{66} shows a large variation of 50 % ($\frac{\Delta C_{66}}{C_{66}}$) as the temperature is reduced to $T_{N1} \simeq 14 \text{ K}$. This large variation

in the value of C_{66} indicates that some of the acoustic modes in CuFeO_2 substantially soften close to 14 K. Similar softening is also found in ferroelectric compounds ($\text{SrBr}_2(\text{NbTa})_2\text{O}_9$ [20], $\text{Sr}_2\text{Ta}_2\text{O}_9$ [21], KNbO_3 and KTaO_3 [22]), as well as in proper ferroelastic (TeO_2 [23], Na_2CO [24], $(\text{NH})_4\text{LiH}_3(\text{S})_4$ [25], $\text{KBr} : \text{KCN}$ [26]) and pseudo-proper ferroelastic ($\text{Na}_5\text{Al}_3\text{F}_{14}$ [21], $\text{LaP}_5\text{O}_{14}$, $\text{KH}_3(\text{SeO}_3)_2$, [23] $\text{Rb}_4\text{LiH}_3(\text{S})_4$ [27]). In general, this softening can be accounted for by a linear-linear coupling term, such as eQ between the strain e and an order parameter Q . In the case of ferroelectric materials, the order parameter is naturally the electric polarization. For proper ferroelastic compounds the order parameter is rather the strain e associated with the softening of an acoustic mode [24, 26]. Finally, for pseudo-proper ferroelastic transition the order parameter can be associated with a soft optical mode [21, 27].

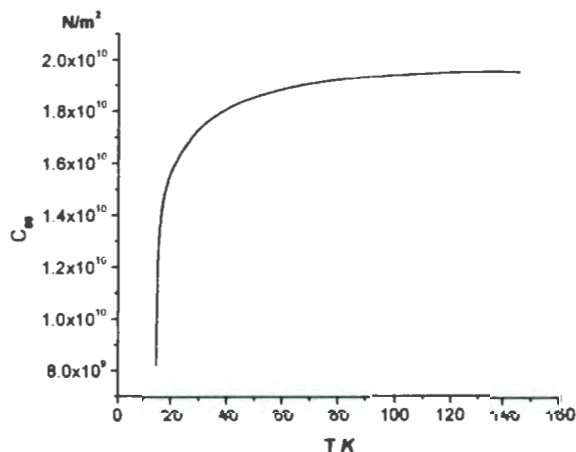


Figure 4.1: Experimental values for the elastic constant C_{66} as a function of temperature for CuFeO_2 .

Since CuFeO_2 shows both structural and magnetic phase transition at T_{N1} [2, 19], it would be natural to assume that the order parameter Q is the spin S . However, as the coupling term eS breaks the time reversal symmetry, this coupling is not allowed and thus the spin moments cannot lead to the observed strong softening on C_{66} . Another possibility would be to assume that the order parameter is associated with an acoustic

mode, which leads to softening at high temperature and a structural transformation observed below T_{N1} . In that case, the transition is called proper ferroelastic and the temperature dependence of the soft-acoustic mode is linear over a wide range [27, 28]. As shown in Fig 4.1, this is not the case for CuFeO_2 . The last scenario is to consider that the softening is driven by a soft-optical mode. In that case, the temperature dependence is non-linear [21, 27] and could potentially account for the temperature dependence of C_{66} , as shown in Fig 4.1. Thus, in this chapter, we derive the free energy assuming that the character of the transition is a pseudo-proper ferroelastic. For this reason, we give a short account of ferroelastic materials.

4.2 Ferroelastics and Ferroelastic Transitions

A crystal is said to be ferroelastic [11, 29] when it has two or more phases (orientation states or structural domains) in the absence of mechanical stress. Any of these structural domains are identical or enantiomorphous (structural mirror images). These domains can be shifted from one to another by mechanical stress. The crystal comes back to its original domain state soon after the removal of the mechanical stress. There is an analogy between ferroelastic and ferromagnetic materials. In a ferromagnetic crystal, the magnetic domains can be shifted from one to another by an external magnetic field. Thus, for a ferroelastic transition the mechanical stress corresponds to the external magnetic field while mechanical strain corresponds to magnetization. A ferroelastic transition is associated with a symmetry breaking spontaneous strain. The symmetry change taking place at a ferroelastic transition is characterized by an elastic tensor that has more independent components in the ferroelastic (low-symmetry) phase than that of the tensor associated with the paraelastic (high-symmetry) phase. Consequently, the high and low temperature phases must belong to different crystal systems (point groups). In Tolédano's paper [23], a detailed list of possible ferroelastic point group changes, along with corresponding macroscopic properties, can be found.

4.3 Landau Free Energy for the $R\bar{3}m \rightarrow C2/m$ Ferroelastic Transition in $CuFeO_2$.

In this section, we derive a Landau free energy for the ferroelastic $R\bar{3}m \rightarrow C2/m$ phase transition. According to group theory, the order parameter associated with a $R\bar{3}m \rightarrow C2/m$ structural transition belongs to a two dimensional irreducible representation E [30], represented by

$$(Q_1, Q_2) = (xy, x^2 - y^2) \quad \text{or} \quad (xz, yz). \quad (4.1)$$

These representations are very useful as they can be used to determine how the order parameter components transform under symmetry operations, even if the exact nature of that order parameter is unknown or undetermined.

Assuming the most general form of a Landau free energy, which includes all possible terms up to fourth order in Q_1 and Q_2 ,

$$\begin{aligned} F_L(Q_1, Q_2) = & A_1 Q_1^2 + A_2 Q_2^2 + A_3 Q_1 Q_2 + b_1 Q_1^3 + b_2 Q_2^3 + c_1 Q_1^2 Q_2 + c_2 Q_1 Q_2^2 + \\ & B_1 Q_1^4 + B_2 Q_2^4 + B_3 Q_1^2 Q_2^2 + B_4 Q_1^3 Q_2 + B_5 Q_1 Q_2^3, \end{aligned} \quad (4.2)$$

the allowed terms can be identified by applying the symmetry operations associated with the high temperature $R\bar{3}m$ point group. In fact, it is sufficient to only consider operations associated with the generators of this point group. Thus, the invariant terms can be identified using the symmetry operation (C_{2x}, C_{3z}) which correspond to a 180° rotation around x-axis and a 120° rotation around z-axis. Thus, under these generator operations, it is easy to show that the order parameter components must transform as shown in Table 4.1. For example, according to the Table 4.1, the contribution term $Q_1 Q_2$ is not allowed, so $A_3 = 0$. When we apply all transformation relations given in Table 4.1, the Landau Free energy 4.2 reduces to

$$F_L(Q_1, Q_2) = \frac{1}{2} A(Q_1^2 + Q_2^2) + \frac{1}{3} b(Q_2^3 - 3Q_1^2 Q_2) + \frac{1}{4} B(Q_1^2 + Q_2^2)^2, \quad (4.3)$$

which is identical to the result published by Tolédano[23].

Table 4.1: Cartesian coordinate representations of the order parameters and the corresponding transformations under space group generators

	Q_1	Q_2
	xy	$x^2 - y^2$
C_{2x}	$-Q_1$	Q_2
C_{3z}	$\frac{\sqrt{3}}{4} Q_2 - \frac{1}{2} Q_1$	$-\frac{1}{2} Q_2 - \sqrt{3} Q_1$

4.4 Derivation of the Model

In order to calculate the variation in the elastic properties associated with a $R\bar{3}m \rightarrow C2/m$ structural phase transition, the free energy must contain terms involving order parameters, the elastic energy, and the coupling energy due to the coupling between the order parameters and strains. Thus, the total free energy can be written as

$$F(e, Q) = F_l(Q) + F_e(e) + F_c(e, Q). \quad (4.4)$$

As discussed, the Landau free energy for $R\bar{3}m \rightarrow C2/m$ structural phase transition is given by (4.3) with $A = a_1(T - T_\theta)$. Here T_θ defines the transition temperature in the absence of elastic coupling. As we noted in Chapter 3 section 3.4, the above Landau free energy (4.3) is a 2-3-4 potential. Consequently, the phase transition observed at T_{N1} should be first order or weakly first order. However, based on the experimental data, the transition at 14 K shows no indication of any discontinuity or hysteresis. Therefore, we simplify the analysis and set the third order coefficient in Landau free energy to zero. So the considered Landau free energy becomes

$$F_L(Q_1, Q_2) = \frac{1}{2} a_1 (T - T_\theta) (Q_1^2 + Q_2^2) + \frac{1}{4} B (Q_1^2 + Q_2^2)^2. \quad (4.5)$$

In Chapter 2, we derived the elastic energy Eq.(2.30) for our model

$$F_e(e_i) = \frac{1}{2} C_p (e_1 + e_2)^2 + \frac{1}{2} C_{33} e_3^2 + \frac{1}{2} C_{44} (e_4^2 + e_5^2) + \frac{1}{2} C_{66} e_6^2 + \frac{1}{2} C_{66} (e_1 - e_2)^2 + C_{13} (e_1 + e_2) e_3 + C_{14} (e_1 e_4 - e_2 e_4 + e_5 e_6) \quad (4.6)$$

where $C_p = \frac{C_{11} + C_{12}}{2}$.

Table 4.2: Strains under the generators

Strains	C_{2x}	C_{3z}
$e_1 (x^2)$	e_1	$\frac{e_1}{4} + \frac{3e_2}{4} - \frac{\sqrt{3}e_6}{4}$
$e_2 (y^2)$	e_2	$\frac{3e_1}{4} + \frac{e_2}{4} + \frac{\sqrt{3}e_6}{4}$
$e_3 (z^2)$	e_3	e_3
$e_4 (yz)$	e_4	$-\frac{e_4}{2} - \frac{\sqrt{3}e_5}{2}$
$e_5 (zx)$	$-e_5$	$\frac{\sqrt{3}e_4}{2} - \frac{e_5}{2}$
$e_6 (xy)$	$-e_6$	$\frac{\sqrt{3}e_1}{2} - \frac{\sqrt{3}e_2}{2} - \frac{e_6}{2}$

Finally, we need to include the coupling energy terms between the strain and the order parameter. Because the high temperature phase has $R\bar{3}m$ symmetry and this structural phase transition is ferroelastic, the order parameter component Q_1 transforms as e_6 and e_5 while Q_2 must transform as $e_1 - e_2$ and e_4 [15, 23]. Here, we consider only two type of coupling terms, they are linear-linear coupling $Q_i e_j$ and linear-quadratic coupling $Q_i^2 e_j$. For linear-linear coupling terms, $Q_1 e_3$, $Q_1 e_4$, $Q_2 e_5$, $Q_2 e_6$ are not allowed by symmetry operations (see Tables 4.1 and 4.2), but coupling terms $Q_1 e_5$, $Q_1 e_6$, $Q_2 (e_1 - e_2)$, $Q_2 e_4$ are allowed with symmetry invariant combinations $Q_2 (e_1 - e_2) + Q_1 e_6$ and $Q_1 e_5 + Q_2 e_4$ [15, 23]. For convenience, we can combine these linear-linear coupling term combinations with two coefficients β_3 and λ in the form $\beta_3(Q_1(e_6 + \lambda e_5) + Q_2(e_1 - e_2 + \lambda e_4))$. For linear-quadratic coupling terms, we can see that only two linear-quadratic coupling terms $\beta_1(Q_1^2 + Q_2^2)e_3$ and $\beta_2(Q_1^2 + Q_2^2)(e_1 + e_2)$ are allowed by symmetry operations (see Tables 4.1 and 4.2). So, the lower coupling terms considered for our model have an energy given by:

$$F_c(e, Q) = \beta_1(Q_1^2 + Q_2^2)e_3 + \beta_2(Q_1^2 + Q_2^2)(e_1 + e_2) + \beta_3(Q_1(e_6 + \lambda e_5) + Q_2(e_1 - e_2 + \lambda e_4)). \quad (4.7)$$

where $\beta_1, \beta_2, \beta_3$ and λ represent the coupling constants.

The equations which minimize $F(e, Q)$ Eq. 4.4 with respect to strains and order parameters are:

$$\frac{\partial F}{\partial e_\alpha} = 0 \quad \text{for } \alpha = 1, \dots, 6. \quad (4.8)$$

$$\frac{\partial F}{\partial Q_\beta} = 0 \quad \text{for } \beta = 1, 2. \quad (4.9)$$

General solutions of equations (4.8) in terms of order parameters Q_1 and Q_2 are:

$$\begin{aligned} e_1 + e_2 &= -2 \frac{(Q_1^2 + Q_2^2)(\beta_1 C_{13} - \beta_2 C_{33})}{C_{13}^2 - C_p C_{33}} \\ e_1 - e_2 &= 2 \frac{Q_2 \beta_3 (\lambda C_{14} - C_{44})}{C_{14}^2 - C_{44} C_{66}} \\ e_3 &= \frac{(Q_1^2 + Q_2^2)(\beta_1 C_p - \beta_2 C_{13})}{C_{13}^2 - C_p C_{33}} \\ e_4 &= \frac{Q_2 \beta_3 (-C_{14} + \lambda C_{66})}{C_{14}^2 - C_{44} C_{66}} \\ e_5 &= \frac{Q_1 \beta_3 (-C_{14} + \lambda C_{66})}{C_{14}^2 - C_{44} C_{66}} \\ e_6 &= \frac{Q_1 \beta_3 (-C_{44} + \lambda C_{14})}{C_{14}^2 - C_{44} C_{66}} \end{aligned} \quad (4.10)$$

Solving equations (4.10) lead three possible sets of solutions for the order parameters Q_1 and Q_2 .

(i) $Q_1 = Q_2 = 0$.

(ii) $Q_1 = 0$ and $Q_2 \neq 0$.

(iii) $Q_1 \neq 0$ and $Q_2 \neq 0$.

Case (i) corresponds to the high temperature $R\bar{3}m$ paraelastic phase. For case (ii), strains e_5 and e_6 are zero, which means that there is no elastic deformation along the xz and xy planes. But other strains e_1, e_2, e_3 and e_4 are non zero, which means that there are elastic deformations along x, y, z axes and yz plane. This changes the length of the crystal axes and the shape of the structure that corresponds to monoclinic symmetry.

Changes in the basal plane associated with e_1 and e_2 , are shown in Fig. 4.2. So case (ii) corresponds to the phase transition from Trigonal to Monoclinic ($R\bar{3}m \rightarrow C2/m$). This is the case we are going to discuss here. Case (iii) corresponds a transition from a high temperature $R\bar{3}m$ trigonal phase to a low temperature $\bar{1}$ triclinic phase.

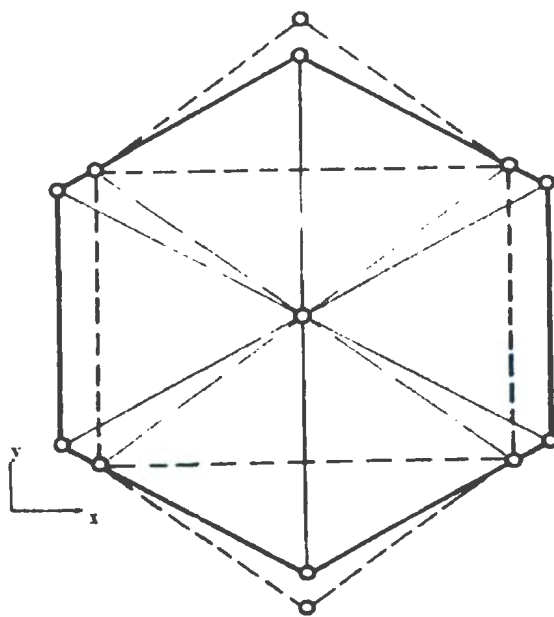


Figure 4.2: Structural phase transition in CuFeO_2 : $R\bar{3}m$ represented by solid lines and $C2/m$ represented by broken lines [31].

For the $R\bar{3}m \rightarrow C2/m$ transition in CuFeO_2 , the complete solution set (case (ii)) can be written as follows:

$$\begin{aligned}
 Q_1 &= 0 \\
 Q_2 &\neq 0 \\
 e_1 + e_2 &= 2 \frac{Q_2^2 (\beta_1 C_{13} - \beta_2 C_{33})}{C_{13}^2 - C_p C_{33}} \\
 e_1 - e_2 &= 2 \frac{Q_2 \beta_3 (-\lambda C_{14} + C_{44})}{C_{14}^2 - C_{44} C_{66}}
 \end{aligned}$$

$$\begin{aligned}
e_3 &= \frac{Q_2^2(-\beta_1 C_p + \beta_2 C_{13})}{C_{13}^2 - C_p C_{33}} \\
e_4 &= \frac{Q_2 \beta_3(-C_{14} + \lambda C_{66})}{C_{14}^2 - C_{44} C_{66}} \\
e_5 &= 0 \\
e_6 &= 0
\end{aligned} \tag{4.11}$$

Next, we need to calculate the critical temperature T_c (T_c is the transition temperature from high temperature phase to low temperature phase). To calculate it, we first substitute the above solutions (4.11) into our total free energy (4.4). This will give that the total free energy expression (4.4) depends only on Q_2 . Which is $F(Q_2)$ given by

$$\begin{aligned}
F(Q_2) &= \frac{Q_2^2(a_1(T - T_\theta)(C_{14}^2 - C_{44}C_{66}) + \beta_3^2(-2\lambda C_{14} + \lambda^2 C_{66} + C_{44}))}{2(C_{14}^2 - C_{44}C_{66})} + \\
&\quad \frac{Q_2^4(2C_p\beta_1^2 - 4\beta_1\beta_2C_{13} + B C_{13}^2 + (B C_p + 2\beta_1^2)C_{33})}{4(C_{13}^2 - C_p C_{33})}
\end{aligned} \tag{4.12}$$

As we discussed in Chapter 3, section 3.3.1, the above energy expression clearly shows that transition is second order. Let us now calculate the transition temperature T_c . First, we differentiate $F(Q_2)$ with respect to Q_2 , and find

$$a_1(T - T_\theta)Q_2 + B Q_2^3 + 2 \frac{Q_2^2(C_p\beta_1^2 + 2\beta_1\beta_2C_{13} - \beta_1^2 C_{33})}{C_{13}^2 - C_p C_{33}} - \frac{Q_2 \beta_3^2(-2\lambda C_{14} + \lambda^2 C_{66} + C_{44})}{C_{14}^2 - C_{44}C_{66}} = 0. \tag{4.13}$$

Therefore at temperature $T = T_c$ the order parameter Q_2 goes to zero. Using this fact in equation (4.13) leads to an expression for T_c which is

$$T_c - T_\theta = \frac{-\beta_3^2(-2\lambda C_{14} + C_{44} + \lambda^2 C_{66})}{a_1 C_{14}^2 - C_{44}C_{66}}. \tag{4.14}$$

4.5 Effective Elastic Constants

In this section, we derive the temperature dependence of the (effective) elastic constants for the trigonal and monoclinic phases. We show how the elastic constants can be obtained from a Landau free energy, defined as a function of a multi-component

order parameter and strains. First, we consider the simplest case where the free energy is only a function of strains ($F(e_i)$), with the effective elastic constants C_{ij} given by

$$C_{ij} = \frac{\partial^2 F}{\partial e_i \partial e_j}. \quad (4.15)$$

Next, we consider the case where the free energy is a function of a multi-component order parameter and strains ($F(e_i, Q_j)$). As the order parameters Q_j and strains e_i are coupled, we must use the chain rule. In that case, the effective elastic constants C_{ij} can be obtained using the following mathematical calculations, where C_{ij} is given by

$$C_{ij} = \frac{\partial^2 F}{\partial e_i \partial e_j} + \sum_m \frac{dQ_m}{de_i} \frac{\partial^2 F}{\partial Q_m \partial e_j} \quad (4.16)$$

We have to eliminate terms $\frac{dQ_m}{de_i}$ in order to get the formula for C_{ij} .

At equilibrium: $\frac{\partial F}{\partial Q_m} = 0$. So, the condition $\frac{d}{de_i} \left(\frac{\partial F}{\partial Q_m} \right) = 0$ leads to

$$\frac{\partial^2 F}{\partial e_i \partial Q_m} + \sum_n \frac{dQ_n}{de_i} \frac{\partial^2 F}{\partial Q_m \partial Q_n} = 0 \quad (4.17)$$

For convenience, let us introduce the following notation:

$$R_{m,i} \equiv \frac{dQ_m}{de_i}, \quad F_{Q_m Q_n} = \frac{\partial^2 F}{\partial Q_m \partial Q_n}, \quad F_{Q_m e_i} = \frac{\partial^2 F}{\partial Q_m \partial e_i}, \quad C_{ij}^o = \frac{\partial^2 F}{\partial e_i \partial e_j}.$$

Using this notation, equations (4.16) and (4.17) become

$$C_{ij} = C_{ij}^o + \sum_m R_{m,i} F_{Q_m e_j}. \quad (4.18)$$

$$F_{Q_m e_i} + \sum_n R_{n,i} F_{Q_m Q_n} = 0. \quad (4.19)$$

These two sets of equations can be solved in order to obtain effective elastic constants.

For this project, as we have two order parameters, Q_1 and Q_2 , we get

$$C_{ij} = C_{ij}^o + \frac{1}{D} \left[-F_{Q_1 e_i} F_{Q_1 e_j} F_{Q_2 Q_2} - F_{Q_2 e_i} F_{Q_2 e_j} F_{Q_1 Q_1} + 2 F_{Q_2 e_i} F_{Q_1 e_j} F_{Q_1 Q_2} \right]. \quad (4.20)$$

where $D = F_{Q_1 Q_1} F_{Q_2 Q_2} - F_{Q_1 Q_2}^2$. Equation (4.20) has been used with the free energy (4.4) in order to calculate the effective elastic constants. The results are conveniently given in Table (4.3) in term of $A(T)$ and the order parameter $Q_2 = Q$ by defining

$$\begin{aligned}
 A(T) &= a_1(T - T_\theta) \\
 Y_+ &= 2Q\beta_2 + \beta_3 \\
 Y_- &= 2Q\beta_2 - \beta_3 \\
 Z_1(Q, T) &= A(T) + \Omega \\
 Z_2(Q, T) &= A(T) + 3BQ^2 + \Omega \\
 \Omega &= \frac{2Q^2(2\beta_1\beta_2C_{13} - \beta_1^2C_p - \beta_2^2C_{33})}{-C_{13}^2 + C_pC_{33}}
 \end{aligned} \tag{4.21}$$

4.6 Experimental Results

The principal elastic constants of CuFeO_2 are obtained using the experimental ultrasonic sound velocity measurements provided by Dr. G. Quirion at Memorial University. The relationships between these velocities and the elastic constants for any corresponding acoustic modes can be derived using Christoffel equations [12], which we discussed in Chapter 2. In Table 4.4, we list the important principal modes, which can be used to calculate the principal elastic constants of CuFeO_2 . The complete list can be found in Chapter 2 (Ref. Tables 2.1 and 2.2).

Table 4.3: Effective elastic constants for both phases of CuFeO_2 .

Elastic Constant	Trigonal ($R\bar{3}m$)	Monoclinic ($C/2m$)
C_{11}	$C_{11}^o - \frac{\beta_3^2}{A(T)}$	$C_{11}^o - \frac{Y_+(Q)^2}{Z_1(Q, T)}$
C_{12}	$C_{12}^o + \frac{\beta_3^2}{A(T)}$	$C_{12}^o - \frac{Y_+(Q)Y_-(Q)}{Z_1(Q, T)}$
C_{13}	C_{13}^o	$C_{13}^o - \frac{2Q\beta_1 Y_+(Q)}{Z_1(Q, T)}$
C_{14}	$C_{14}^o - \lambda \frac{\beta_3^2}{A(T)}$	$C_{14}^o - \frac{\lambda\beta_3 Y_+(Q)}{Z_1(Q, T)}$
C_{22}	$C_{11}^o - \frac{\beta_3^2}{A(T)}$	$C_{11}^o - \frac{Y_-(Q)^2}{Z_1(Q, T)}$
C_{23}	C_{13}^o	$C_{13}^o - \frac{2Q\beta_1 Y_-(Q)}{Z_1(Q, T)}$
C_{24}	$-C_{14}^o + \lambda \frac{\beta_3^2}{A(T)}$	$-C_{14}^o - \frac{\lambda\beta_3 Y_-(Q)}{Z_1(Q, T)}$
C_{33}	C_{33}^o	$C_{33}^o - \frac{4Q^2\beta_1^2}{Z_1(Q, T)}$
C_{34}	0	$-\frac{2Q\beta_1\beta_3\lambda}{Z_1(Q, T)}$
C_{43}	0	$\frac{2Q\beta_1\beta_3\lambda}{Z_1(Q, T)}$
C_{44}	$C_{44}^o - \lambda^2 \frac{\beta_3^2}{A(T)}$	$C_{44}^o - \frac{\lambda^2\beta_3^2}{Z_1(Q, T)}$
C_{55}	$C_{44}^o - \lambda^2 \frac{\beta_3^2}{A(T)}$	$C_{44}^o - \frac{\lambda^2\beta_3^2}{Z_2(Q, T)}$
C_{56}	$C_{14}^o - \lambda \frac{\beta_3^2}{A(T)}$	$C_{14}^o - \frac{\lambda\beta_3^2}{Z_2(Q, T)}$
C_{66}	$C_{66}^o - \frac{\beta_3^2}{A(T)}$	$C_{66}^o - \frac{\beta_3^2}{Z_2(Q, T)}$

Table 4.4: Expression of ρv^2 for trigonal and monoclinic phases

Acoustic modes	Dir./Pol.	Trigonal $R\bar{3}m$ phase	Monoclinic $C/2m$ phase
[100]	Lx [100]	C_{11}	C_{11}
	$Ty \sim [010]$	$\frac{1}{2} (C_{44} + C_{66} - \sqrt{(C_{44} - C_{66})^2 - 4C_{14}^2})$	$\frac{1}{2} (C_{55} + C_{66} + \sqrt{(C_{55} - C_{66})^2 - 4C_{56}^2})$
[010]	Tx [100]	C_{66}	C_{66}
[001]	Lz [001]	C_{33}	$\frac{1}{2} (C_{33} + C_{44} + \sqrt{(C_{33} - C_{44})^2 - 4C_{34}^2})$
	Tx [100]	C_{44}	C_{55}

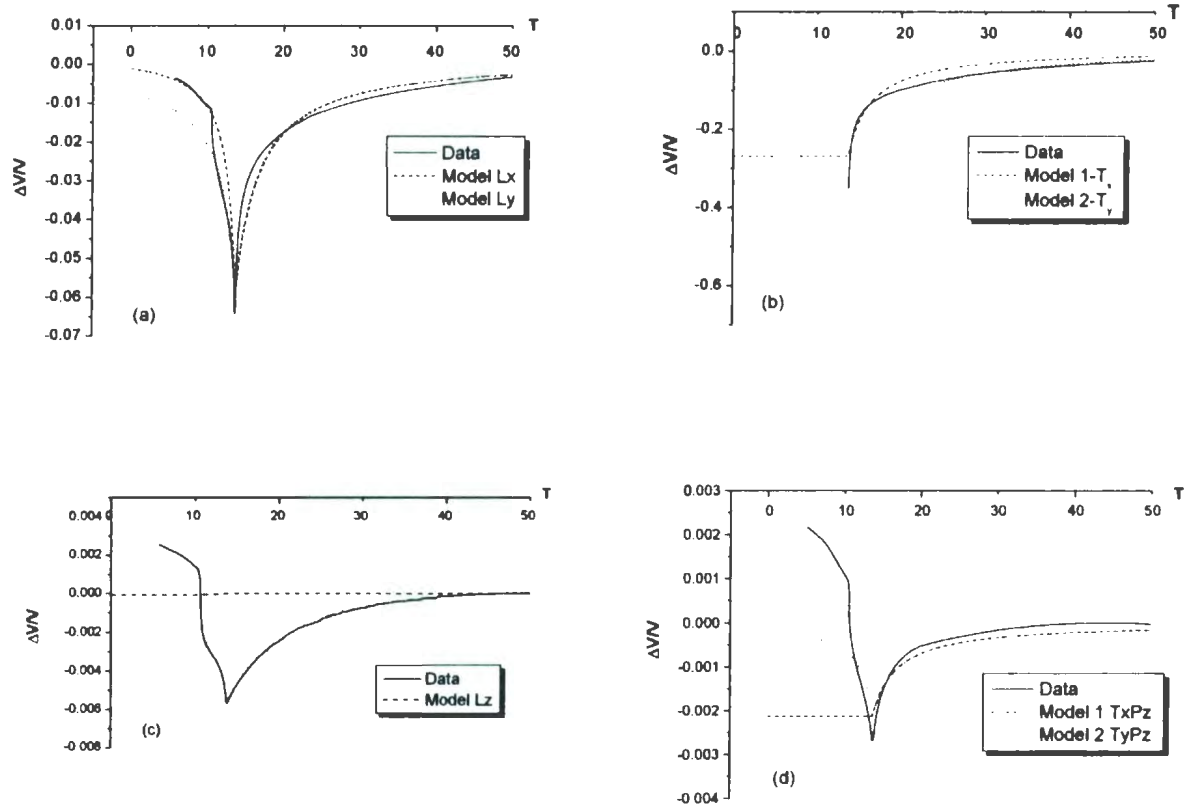


Figure 4.3: Normalized Velocity Plots: (a) $\Delta V_{Lx}/V_{Lx}$ (C_{11}), (b) $\Delta V_{Tx}(P_y)/V_{Tx}(P_y)$ (C_{66}), (c) $\Delta V_{Lz}/V_{Lz}$ (C_{33}), (d) $\Delta V_{Tx}(P_z)/V_{Tx}(P_y)$ (C_{44}) - We are using a different scale for each plot in order to show the good compatibility of the model and data.

The temperature dependence of the relative variation of the velocity $\Delta v/v$ measurement data was taken for the five modes (listed in Table 4.4) between 4 and 300 K. In Fig. 4.3, we present the temperature dependence of the relative variation of the velocity $\Delta v/v$ measurement results from 4 K to 50 K. For convenience, all velocity curves have been normalized relative to the maximum value observed around 100 K. We observed from Fig. 4.3 that there are two distinct anomalies at $T_{N1} = 13.7$ K and

$T_{N2} = 10.6 K$. These temperatures coincide very well with the zero-field magnetic and structural phase transition temperatures observed previously in specific heat, magnetization [8], X-ray [15, 19], and neutron diffraction [8, 32] experiments. At T_{N2} , a thermal hysteresis at $\Delta T = 0.5K$ is observed in the experimental measurement of all modes [1]. This shows that the transition at T_{N2} is weakly first order. Above T_{N1} , we observe that the velocity of all modes presented in Fig. 4.3 increase non-linearly as a function of temperature. This observation alone is a good indicator that the anomalies observed at T_{N1} are associated with a pseudo-proper ferroelastic transition [23, 27]. The observed softening on C_{66} is also very large, almost 50%. At the same time, the softening on C_{33} and C_{44} is at least two orders of magnitude smaller, shown in Fig. 4.3c and Fig. 4.3d. Finally, Figs. 4.3a and 4.3b (note difference in scale) indicate that the softening on C_{11} is small compare to C_{66} , nevertheless it is significant as V_{Lx} shows a decrease of 6.5% at T_{N1} .

4.7 Numerical Calculation and Model fitting to Ultrasonic Experimental Data on CuFeO_2

4.7.1 Numerical Calculation

The absolute sound velocities of longitudinal waves (propagating along x and z directions) and for transverse waves (propagating along x direction) have been measured at room temperature [1] (see Table 4.5).

Table 4.5: Velocity values at $T = 300 K$

Velocity propagation	V_{Lx}^o	V_{Lz}^o	$V_{Tx}(P_z)^o$	$V_{Tx}(P_y)^o$
(m/s)	3767	4400	1400	1900

The relationships between velocity and elastic constant for each mode are given by

$$\begin{aligned}
 C_{11}[T] &= \rho V_{Lx}^2[T] \\
 C_{33}[T] &= \rho V_{Lz}^2[T] \\
 C_{44}[T] &= \rho V_{Tz}(P_x)^2[T] \\
 C_{66}[T] &= \rho V_{Ty}(P_x)^2[T].
 \end{aligned} \tag{4.22}$$

The density of CuFeO_2 is $\rho = 5410 \text{ kg/m}^3$. We can use these equations 4.22 and the velocity values listed in Table 4.5 to find some of the bare elastic constants (C_{11} , C_{12} , C_{33} , C_{44} , C_{66}). To calculate C_{14} , we have to find a_1 and λ . For convenience, we fixed $a_1 = 1$, and then try a number of values for λ in order to get the best model fit for the ultrasonic experimental velocity data V_{Lx} on CuFeO_2 for the temperature range from 0 to 100K. This leads to $\lambda = 0.07$. We use experimental values of velocity V_{Lx} (which is $V_{Lx}(T_c) = 0.938 \times V_{Lx}^o$ see Fig: 4.3a) and the elastic constant C_{11} at $T = T_c$ and first equation of (4.22) to calculate C_{14} . Next we use again experimental values of velocity V_{Lx} (which is $V_{Lx}(15) = 0.965 \times V_{Lx}^o$) and the elastic constant C_{11} at $T = 15 \text{ K}$ and the first equation of (4.22) to calculate β_3 . Using bare elastic constant values listed in Table 4.6 and the values of a_1 , λ , β_3 listed in Table 4.7, we can find the elastic tensor matrix at high temperature (above T_c). Next, we can determine some strain values at $T = 0 \text{ K}$: $e_1(0) = -0.0024$, $e_2(0) = +0.0026$, $e_3(0) = 0.00001$. First we use $e_1(0) - e_2(0)$ and the fourth equation of (4.11) to find $Q_2(0)$, then we use $Q_2(0)$, $e_3(0)$ and $e_1(0) + e_2(0)$ (see complete values set in Table 4.8) and the equations from (4.11) to find rest of the β_1 , β_2 , B (see Table 4.7). Using all these values, we can find the elastic tensor matrix at low temperature (below T_c).

4.7.2 Summary of the calculation and model fitting of the data

The following values are calculated for our model. Table 4.6 shows the elastic constants at 300 K. Coupling constants and other variable values resulting from the fit to the data are listed in Table 4.7. Strains and order parameters values at $T = 0 \text{ K}$ are in the

Table 4.6: Elastic Constants at $T = 300 K$

Elastic Constant	C_{11}	C_{12}	C_{13}	C_{14}	C_{33}	C_{44}	C_{66}
$\times 10^{10} (N/m)$	7.68	3.77	1.89	1.11	10.47	1.06	1.95

Table 4.7: Coupling/other constants

Coupling/other Constant	a_1	B	β_1	β_2	β_3	λ
(N/m)	1	1	-90.52	-182.21	238320	0.07

Table 4.8: Strains (S) and order parameters (OP) values at $T = 0 K$

S/OP	e_1	e_2	e_3	e_4	e_5	e_6	Q_1	Q_2
	- 0.0024	0.0026	0.00001	0.005	0	0	0	180.14

Table 4.9: Other values: mass density, critical temperature.

T_c	T_θ	$T_c - T_\theta$	ρ
13.7 K	10.6214 K	3.07862 K	5410 kg/m ³

Table 4.8. Let us first plot the order parameters and strains. The plot of the order parameter Q_2 (see Fig. 4.4) verifies that our transition is continuous (second order transition). This agrees with the solution of Q_2 (see second equation of (4.11)). The plots of strains e_m and e_4 exhibit temperature dependence like Q_2 and verifies that our transition is second order. The plots of strains e_p and e_3 exhibit a linear dependence of temperature (see Fig. 4.5) as these solutions depend on Q_2^2 (see equations of (4.11)).

Next, we will focus on the ultrasonic experimental data and model plots of the normalized velocity vs temperature (see Fig. 4.3). Our first plot in Fig. 4.3 (a) is the normalized velocity data for longitudinal modes along the x and y directions. The solid line is our data and the dashed and dotted dashed lines are from the model along

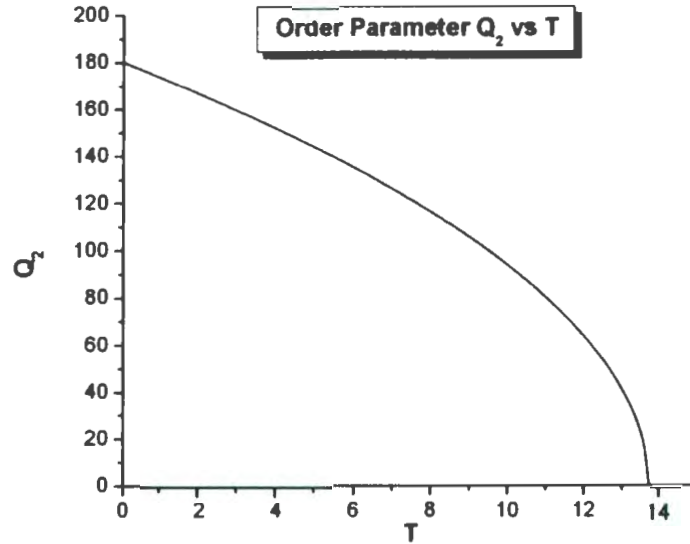


Figure 4.4: Plot of the order parameter Q_2 , equation (4.6)

the x and y directions of the longitudinal modes. We notice from this fit that there are two phase transitions. One is at about 10K and the other one about 13.7K. We can also see from the Fig. 4.3 (a) that the longitudinal waves propagating along [100] with a [100] polarization (V_{Lx}) agree very well with our experimental data. Both directions (x and y) of polarizations agree with data above T_c . The second plot in Fig. 4.3 (b) corresponds to $V_{Tx}(P_y)$. Here the dashed line of the model exhibits the soft mode ($\Delta V/V \simeq 80\%$) behavior. This is also seen in Fig. 4.3 (a). Unfortunately, due to large acoustic attenuation for that particular mode, we were unable to obtain data in the ferroelastic phase below 13 K. The third plot Fig. 4.3 (c) corresponds to V_{Lz} , here we did not see any agreement between data and experiment above $T_c \simeq 14$ K. There is deviation between the model and data for low temperature part. However, we notice from the scale of Fig. 4.3 (c) that $\Delta V_{Lz}/V_{Lz} \leq 1\%$. The anomaly in Fig. 4.3 (c) is shown in the next chapter 5 to be due to magnetoelastic coupling. Our fourth plot in

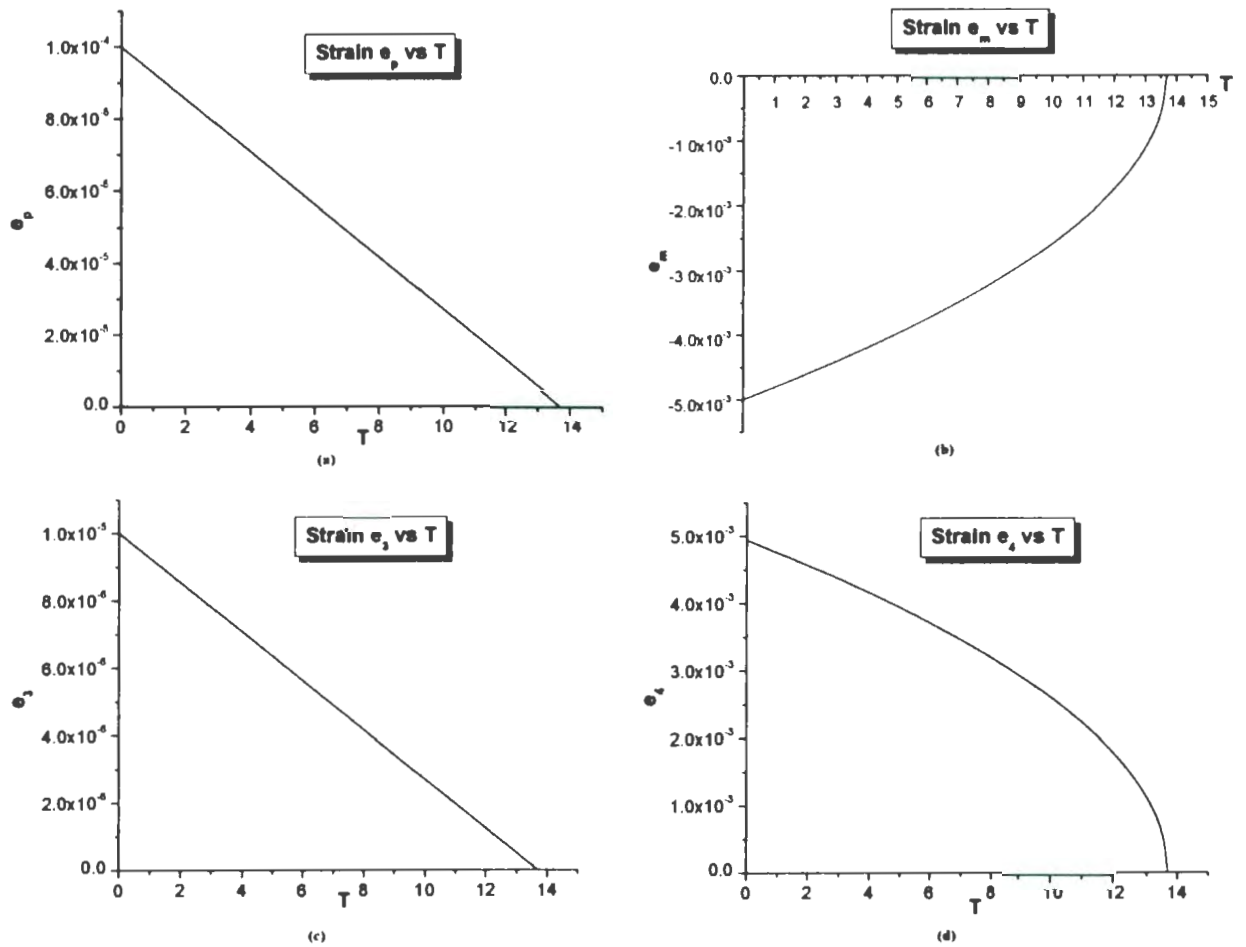


Figure 4.5: Temperature dependence of the strains. Plots correspond to the equation (4.6): (a) $e_p = \frac{e_1 + e_2}{2}$, (b) $e_m = \frac{e_1 - e_2}{2}$, (c) e_3 , (d) e_4

Fig. 4.3 (d) corresponds to $V_{Tx}(P_z)$. The model (transverse wave propagation along [001] with a [010] polarization) shows by dotted line agrees with the data for both low and high temperature. We see from all data plots except the soft mode, there is another transition about 10K. Anomalies in these modes are also visible, and variations near critical point are small order in magnitude.

The overall good quality of the model fit to experimental data for $\Delta V_{Lz}/V_{Lz}^o$ and $\Delta V_{Tx}(P_y)/V_{Tx}(P_y)^o$, which exhibit nearly soft mode behavior, suggest that our theory captures the essential features of the ferroelastic phase transition in CuFeO_2 . These results have recently been published [1].

As mentioned in the Introduction, CuFeO_2 also exhibits magnetic transitions at $T_{N1} \cong 10 \text{ K}$ and $T_{N2} \cong 14 \text{ K}$, which correspond to the temperatures at which anomalies are seen in the ultrasound data. The possible impact of coupling between elastic and magnetic degrees of freedom is explored in the next chapter.

Chapter 5

Magnetoelastic Coupling

So far, we analyzed the elastic properties of CuFeO_2 using a Landau theory of phase transition which ignores the magnetic degrees of freedom. As shown in Chapter 4, this preliminary model accounts well for the structural phase transition observed at 14 K. However, it fails to reproduce any of the anomalies observed on the velocity measurements at 11 K. In this chapter, we are going to investigate how the magnetoelastic coupling affects the elastic properties of CuFeO_2 . Again, an approach based on a nonlocal Landau free energy functional, as described by Plumer and Caillé [33], is used. First, we consider the spin ordering alone, followed by the derivation of the coupling between the elastic and magnetic degrees of freedom. Finally, the impact of the magnetoelastic effect on the elastic constants C_{ij} is presented.

5.1 Spin Energy

5.1.1 Theoretical Approach

In this section, the free energy, as a functional of the spin density $\mathbf{s}(\mathbf{r})$ is derived at $H = 0$ T. According to neutron diffraction experiments on CuFeO_2 [2, 6] at zero field, all spins align along the c-axis so that the spin polarization is parallel to the z-axis which coincide with the c-direction. Moreover, due to time inversion symmetry, only

even powers of $\mathbf{s}(\mathbf{r})$ are allowed. Consequently, the spin free energy up to fourth order can be expressed as

$$F[\mathbf{s}] = F_{2\mathbf{s}}[\mathbf{s}] + F_{4\mathbf{s}}[\mathbf{s}], \quad (5.1)$$

where the second order spin contribution is

$$F_{2\mathbf{s}} = \frac{1}{2V} \int d\mathbf{r}_1 d\mathbf{r}_2 J_{\alpha\beta}(\mathbf{r}_1, \mathbf{r}_2) s_\alpha(\mathbf{r}_1) s_\beta(\mathbf{r}_2), \quad (5.2)$$

with the fourth order contribution given by

$$F_{4\mathbf{s}} = \frac{1}{4V} \int d\mathbf{r}_1 d\mathbf{r}_2 d\mathbf{r}_3 d\mathbf{r}_4 B_{\alpha\beta\gamma\delta}(\mathbf{r}_1, \mathbf{r}_2, \mathbf{r}_3, \mathbf{r}_4) s_\alpha(\mathbf{r}_1) s_\beta(\mathbf{r}_2) s_\gamma(\mathbf{r}_3) s_\delta(\mathbf{r}_4). \quad (5.3)$$

Here, the summation convention has been used with $\alpha, \beta, \gamma, \delta = x, y, z$ with V representing the volume of the crystal. Knowing that the space group of CuFeO_2 is $R\bar{3}m$, we impose that the free energy (5.1) remains invariant under the symmetry operations of the group generators C_{2x} and C_{3z} . Using this argument, the second order terms (5.2) can be written as

$$F_{2\mathbf{s}} = \frac{1}{2V} \int d\mathbf{r}_1 d\mathbf{r}_2 J(\mathbf{r}_1, \mathbf{r}_2) \mathbf{s}(\mathbf{r}_1) \cdot \mathbf{s}(\mathbf{r}_2) + \frac{1}{2V} \int d\mathbf{r}_1 d\mathbf{r}_2 J_z(\mathbf{r}_1, \mathbf{r}_2) s_z(\mathbf{r}_1) s_z(\mathbf{r}_2), \quad (5.4)$$

and the fourth order spin energy (5.3) can be expressed as

$$\begin{aligned} F_{4\mathbf{s}} = & \frac{1}{4V} \int d\mathbf{r}_1 d\mathbf{r}_2 d\mathbf{r}_3 d\mathbf{r}_4 \tilde{B}(\mathbf{r}_1, \mathbf{r}_2, \mathbf{r}_3, \mathbf{r}_4) \mathbf{s}(\mathbf{r}_1) \cdot \mathbf{s}(\mathbf{r}_2) \mathbf{s}(\mathbf{r}_3) \cdot \mathbf{s}(\mathbf{r}_4) + \\ & \frac{1}{4V} \int d\mathbf{r}_1 d\mathbf{r}_2 d\mathbf{r}_3 d\mathbf{r}_4 B_{z1}(\mathbf{r}_1, \mathbf{r}_2, \mathbf{r}_3, \mathbf{r}_4) \mathbf{s}(\mathbf{r}_1) \cdot \mathbf{s}(\mathbf{r}_2) s_z(\mathbf{r}_3) s_z(\mathbf{r}_4) + \\ & \frac{1}{4V} \int d\mathbf{r}_1 d\mathbf{r}_2 d\mathbf{r}_3 d\mathbf{r}_4 B_{z2}(\mathbf{r}_1, \mathbf{r}_2, \mathbf{r}_3, \mathbf{r}_4) s_z(\mathbf{r}_1) s_z(\mathbf{r}_2) s_z(\mathbf{r}_3) s_z(\mathbf{r}_4) + \\ & \frac{1}{4V} \int d\mathbf{r}_1 d\mathbf{r}_2 d\mathbf{r}_3 d\mathbf{r}_4 E(\mathbf{r}_1, \mathbf{r}_2, \mathbf{r}_3, \mathbf{r}_4) [3s_x(\mathbf{r}_1) s_x(\mathbf{r}_2) - s_y(\mathbf{r}_1) s_y(\mathbf{r}_2)] s_y(\mathbf{r}_3) s_z(\mathbf{r}_4). \end{aligned} \quad (5.5)$$

Here, J and B are coefficients associated with isotropic contributions while the other constants are related to anisotropic contributions. The fourth order free energy (5.5) can be simplified further using that $\mathbf{s}(\mathbf{r}) \parallel \hat{z} \parallel \hat{c}$ (at $\mathbf{H} = 0$) so that

$$F_{4\mathbf{s}} = \frac{1}{4V} \int d\mathbf{r}_1 d\mathbf{r}_2 d\mathbf{r}_3 d\mathbf{r}_4 \tilde{B}(\mathbf{r}_1, \mathbf{r}_2, \mathbf{r}_3, \mathbf{r}_4) s_z(\mathbf{r}_1) s_z(\mathbf{r}_2) s_z(\mathbf{r}_3) s_z(\mathbf{r}_4), \quad (5.6)$$

where $\tilde{B} = B + B_{z1} + B_{z2}$. Note that $\mathbf{S} \parallel \hat{z} \parallel \hat{c}$, minimizes the free energy (5.1) for $J_z < 0$. For simplicity, we assume that the anisotropy contribution (second term of (5.4)) is of the single-ion form $-D \int d\mathbf{r} [s_z(\mathbf{r})]^2$.

The long range ordering of the magnetic ions can be described by a quantity $\rho(\mathbf{r})$, which is related to the spin density $\mathbf{s}(\mathbf{r})$ [33] by

$$\mathbf{s}(\mathbf{r}) = \frac{V}{N} \sum_{\mathbf{R}} \rho(\mathbf{r}) \delta(\mathbf{r} - \mathbf{R}), \quad (5.7)$$

where \mathbf{R} represents the lattice vectors and N is the number of Fe^{3+} ions. We assume further that $\rho(\mathbf{r})$ [33] can be represented by a single component Fourier expansion

$$\rho(\mathbf{r}) = \mathbf{S} e^{i\mathbf{Q}\cdot\mathbf{r}} + \mathbf{S}^* e^{-i\mathbf{Q}\cdot\mathbf{r}}, \quad (5.8)$$

where \mathbf{S} is the spin polarization vector and \mathbf{Q} represents the wave vector of the modulation restricted to the first Brillouin zone. The polarization vectors for the ABC triangular layers is assumed to have the following form [35]:

$$\mathbf{S}_A = S e^{i\phi} \hat{z}, \quad \mathbf{S}_B = S e^{i(\phi-\gamma)} \hat{z}, \quad \mathbf{S}_C = S e^{i(\phi-\gamma)} \hat{z}, \quad (5.9)$$

where the magnitude S is real and ϕ is an overall phase angle and γ is the phase angle difference between the two adjacent layer stacks. Using (5.7), (5.8) and (5.9) in (5.4), the second order contribution to the free energy reduces to

$$F_{2S} = (A_Q - D)S^2, \quad (5.10)$$

with $A_Q = a_1(T + J_Q)$, where a_1 is a constant, T is the temperature, and J_Q [35] represents the strength of the effective spin-spin coupling given by

$$J_Q = \frac{2}{3}(J_1 f_1 + J_2 f_2 + J_3 f_3 + J' f'). \quad (5.11)$$

As illustrated in Fig. 5.1, J_1 is the near neighbour (NN) in plane (triangular) exchange coupling, J_2 is the 2nd NN coupling in plane, J_3 is the 3rd NN coupling in plane, and J' is the coupling between planes. For this geometry, one finds [35] that f_i , $i = 1, 2, 3$

and f' are given by

$$f_1 = \cos x + 2 \cos \frac{1}{2}x \cos y \quad (5.12)$$

$$f_2 = \cos 2y + 2 \cos \frac{3}{2}x \cos y \quad (5.13)$$

$$f_3 = \cos 2x + 2 \cos x \cos 2y \quad (5.14)$$

$$f' = \frac{1}{3}(1 + 2 \cos \phi) \left[\cos \left(\frac{2}{3}y - \frac{1}{3}z \right) + 2 \cos \frac{1}{2}x \cos \left(\frac{1}{3}y + \frac{1}{3}z \right) \right], \quad (5.15)$$

where $x = aQ_x$, $y = bQ_y$, $z = cQ_z$, and a is the in-plane lattice constant, $b = \frac{\sqrt{3}}{2}a$ and c is the z-axis lattice constant (spanning three triangular layers).

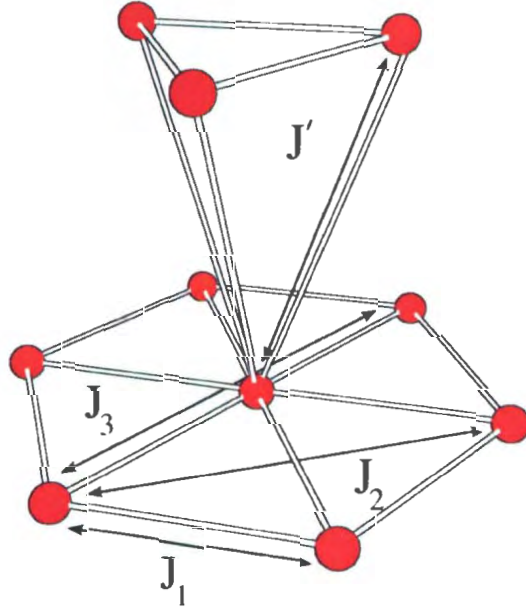


Figure 5.1: Spin-exchange paths J_1 , J_2 and J_3 within an FeO_2 layer (in plane) and spin-exchange path J' between adjacent FeO_2 layers (planes) [34].

Substituting (5.7), (5.8) and (5.9) in (5.6), the fourth order contribution to the free energy can be written as

$$F_{4S} = \hat{B}_Q S^4 + C'_Q S^4 \cos(4\gamma) \Delta_{4\mathbf{Q}, \mathbf{G}}. \quad (5.16)$$

where

$$\begin{aligned}\hat{B}_Q &= \hat{B}_{Q,-Q,Q,-Q} + \frac{1}{2}\hat{B}_{Q,Q,-Q,-Q}, \\ C_Q &= \frac{1}{2}\hat{B}_{Q,Q,Q,Q}.\end{aligned}\quad (5.17)$$

One can find expressions for \hat{B}_Q and C_Q in Ref. [33], while $\Delta_{4\mathbf{Q},\mathbf{G}}$ represents the Kronecker Delta function given by

$$\Delta_{4\mathbf{Q},\mathbf{G}} = \frac{1}{N} \sum_{\mathbf{R}} e^{4i\mathbf{Q}\cdot\mathbf{R}} \quad (5.18)$$

with \mathbf{G} being a reciprocal lattice vector. Substituting (5.10) and (5.16) in (5.1), the free energy can finally be written as

$$F(S) = F_{IC} + F_U \Delta_{4\mathbf{Q},\mathbf{G}}, \quad (5.19)$$

where F_{IC} represents the free energy contribution for an incommensurate modulation,

$$F_{IC} = (A_Q - D)S^2 + B_{IC}S^4, \quad (5.20)$$

where $\hat{B}_Q = B_{IC}$ for the incommensurate modulation \mathbf{Q} . The free energy F_U is associated with the a Umklapp term allowed only for a commensurate modulation associated with $\Delta_{4\mathbf{Q},\mathbf{G}}$, so that

$$F_U = B_C S^4 + C_Q S^4 \cos(4\gamma), \quad (5.21)$$

with $\hat{B}_Q = B_C$. Note that $\mathbf{Q} = \frac{1}{4}\mathbf{G}$ does describe the observed period-4 spin structure for $T < T_{N2}$.

Let us first restrict our analysis to the incommensurate modulation. In this case, the free energy is given by (5.20). Minimizing the free energy with respect to S gives

$$S_{IC}^2 = -\frac{a_1}{2B_{IC}} \left(T + J_Q - \frac{D}{a_1} \right), \quad (5.22)$$

As the transition is continuous, we immediately obtain that $T_{N1} = -J_Q + \frac{D}{a_1}$. Using (5.22) in (5.20), the free energy for an incommensurate modulation is

$$F_{IC} = -\frac{a_1^2(T - T_{N1})^2}{4B_{IC}}. \quad (5.23)$$

For the commensurate modulation, considering that the Umklapp term $\Delta_{4\mathbf{Q},\mathbf{G}} = 1$ and $\gamma = \frac{\pi}{4}$, the free energy reduces to

$$F_C = (A'_Q - D)S^2 + \hat{B}_Q S^4 - C_Q S^4, \quad (5.24)$$

where $A'_Q = a_1(T + J'_Q)$, with J'_Q being calculated using (5.11) for $\mathbf{Q} = \frac{1}{4}\mathbf{G}$, while $\hat{B}_Q = B_{1C} + B_C$. Minimizing with respect to S gives

$$S_C^2 = -\frac{a_1}{2(\hat{B}_Q - C_Q)} \left(T + J'_Q - \frac{D}{a_1} \right). \quad (5.25)$$

We immediately see that, for a continuous phase transition, the order parameter would normally be zero at a temperature $T_o = -J'_Q + \frac{D}{a_1}$. However, as the transition for the commensurate phase is first order, the actual transition temperature has to be obtained by comparing the incommensurate free energy (5.23) with the commensurate free energy F_C given by

$$F_C = -\frac{a_1^2(T - T_o)^2}{4(\hat{B}_Q - C_Q)} \quad (5.26)$$

with the condition that $T_{N2} < T_o < T_{N1}$. Considering that both free energies must be equal at the critical temperature T_{N2} , this leads to the condition that

$$C_Q = \hat{B}_Q - B_{1C} \left(\frac{T_{N2} - T_o}{T_{N2} - T_{N1}} \right). \quad (5.27)$$

5.1.2 Numerical Calculation

For the moment, no experimental results relative to the exchange couplings constants: J_1, J_2, J_3 and J' exist. For that reason, the normalized values used in this work: $J_1 \equiv 1, J_2 = 0.27, J_3 = 0.3$, and $J' = 0.4$, are similar to those used in Ref. [36] in order to reproduce the series of phases observed as a function of the magnetic field at $T = 0$ K. With these values, the wave vector associated with the spin modulation is obtained by minimizing (5.11) with respect to x, y and z . For the incommensurate phase, we obtain

$$\mathbf{Q} = \left(-0.26 \frac{2\pi}{a}, 0.675 \frac{2\pi}{b}, \frac{\pi}{c} \right) \text{ with } J_Q = -0.9776, \quad (5.28)$$

which is consistent with the wave vector of the spin modulation observed by neutron scattering [10]. Setting $a_1 \equiv 1$, $B_{IC} \equiv 1$, and $D \equiv 0.1$ (for convenience) with equations (5.22) and (5.23), we then get

$$S_{IC} = 0.71\sqrt{-1.08 + T}, \quad (5.29)$$

and

$$F_{IC}(T) = -0.25(-1.08 + T)^2. \quad (5.30)$$

From equation (5.29) the transition temperature is $T_{N1} = 1.08$ in units of J_1 .

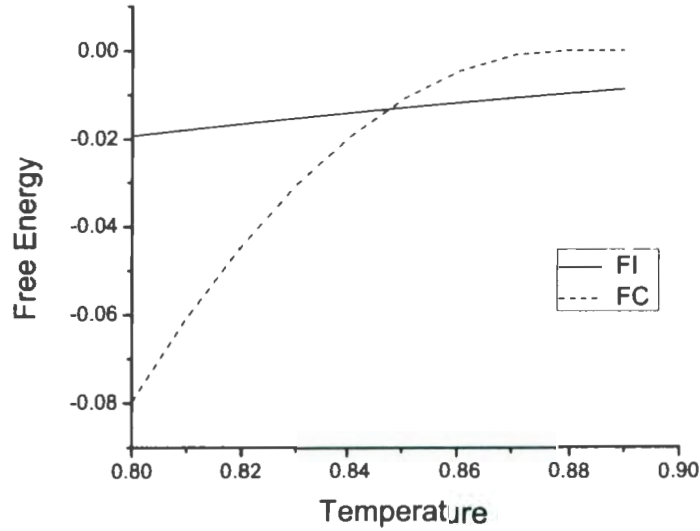


Figure 5.2: Plot of the free energies for incommensurate and commensurate phases. F_{IC} , and F_C represent the equations (5.30) and (5.32), respectively.

Regarding the commensurate phase, as neutron scattering measurements [10] indicate that the wave vector of the spin modulation corresponds to a period-4, we set the x , y and z parameters as $x = \frac{\pi}{2}$, $y = \frac{\pi}{2}$, $z = 0$ with $\phi = 0$ and $\gamma = \frac{\pi}{4}$ [35]. With these values, we then get $J'_C = -0.78$ and $T_o = 0.88$. The constant $C_Q = 1.08$ is determined by setting $\tilde{B}_Q = 1.1$ and imposing the experimental condition that $T_{N2} = \frac{11}{14} T_{N1}$ with

equation (5.27). Substituting all these values into the equations (5.25) and (5.24) we then get

$$S_C = 5.05\sqrt{-0.88 + T}, \quad (5.31)$$

and

$$F_C(T) = -12.73(-0.88 + T)^2. \quad (5.32)$$

The first order transition temperature between incommensurate and commensurate phases is found to be $T_{N2} = 0.85$, which can be determined from Fig. 5.2, where $F_C = F_{IC}$. Combining equations (5.29) and (5.31), the mean field temperature dependence of the spin amplitude is

$$S(T) = \begin{cases} 5.05\sqrt{-0.88 + T}, & T \leq T_{N2}; \\ 0.71\sqrt{-1.08 + T}, & T_{N2} \leq T \leq T_{N1}; \\ 0, & \text{otherwise,} \end{cases} \quad (5.33)$$

where $T_{N1} = 1.08$ and $T_{N2} = 0.85$ are the re-normalized values defined with respect to J_1 . The temperature dependence of $S(T)$ is shown in Fig. 5.3 where the temperature has been rescaled in order to coincide with the observed transition temperatures $T_{N1} = 14 \text{ K}$ and $T_{N2} = 11 \text{ K}$.

5.2 Effect of the Magnetoelastic Coupling

In this section, we are going to determine the magnetoelastic coupling terms and analyze their impact on the elastic properties of CuFeO_2 . For that purpose, the free energy must include the magnetic degrees of freedom (spin density) derived in section 5.1, the elastic energy, derived in section 2.6, and the magnetoelastic coupling energy due to the coupling between the magnetic degrees of freedom (spin density) and strains. Thus, the total free energy can be written as

$$F(e, S) = F_L(S) + F_e(e) + F_{mc}(e, S). \quad (5.34)$$

where $F_L(S)$ corresponds to equation (5.19) and the elastic energy $F_e(e)$ given by equation (2.30). We now derive the allowed coupling terms between the spin density

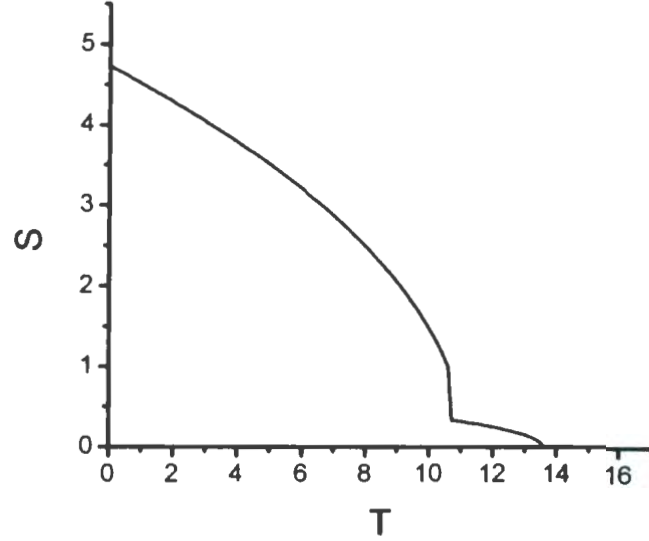


Figure 5.3: Rescaled temperature dependence of the magnetic moment according to equation (5.33).

and strains. For our analysis, we consider two type of magnetoelastic coupling terms, linear-quadratic ($e S^2$) and quadratic-quadratic ($e^2 S^2$). Thus, for our analysis these contributions are represented by

$$F_{mc} = F_{mc}^{lq} + F_{mc}^{qq}, \quad (5.35)$$

where F_{mc}^{lq} and F_{mc}^{qq} are the linear-quadratic and quadratic-quadratic coupling terms, respectively.

The general expressions for the linear-quadratic and quadratic-quadratic coupling energy can be written as

$$F_{mc}^{lq} = \frac{1}{2V} \int d\mathbf{r}_1 d\mathbf{r}_2 d\mathbf{r}_3 K_{\alpha\beta\gamma\delta}(\mathbf{r}_1, \mathbf{r}_2, \mathbf{r}_3) c_{\alpha\beta}(\mathbf{r}_1) s_{\gamma}(\mathbf{r}_2) s_{\delta}(\mathbf{r}_3), \quad (5.36)$$

and

$$F_{mc}^{qq} = \frac{1}{4V} \int d\mathbf{r}_1 d\mathbf{r}_2 d\mathbf{r}_3 d\mathbf{r}_4 M_{\alpha\beta\gamma\delta\zeta\eta}(\mathbf{r}_1, \mathbf{r}_2, \mathbf{r}_3, \mathbf{r}_4) c_{\alpha\beta}(\mathbf{r}_1) c_{\gamma\delta}(\mathbf{r}_2) s_{\zeta}(\mathbf{r}_3) s_{\eta}(\mathbf{r}_4), \quad (5.37)$$

where V is the volume of the crystal. Again, the summation convention is used with $\alpha, \beta, \gamma, \delta, \zeta, \eta = x, y, z$. The invariant terms can be identified by applying the symmetry operations associated with the $R\bar{3}m$ point group as described in section 5.1.1. Both linear-quadratic and quadratic-quadratic coupling terms can be reduced considering that $\mathbf{S} \parallel \hat{z} \parallel \hat{c}$. Thus, the possible terms compatible with the high temperature symmetry correspond to

$$F_{mc}^{lq} = K_1(e_1 + e_2)S^2 + K_2e_3S^2, \quad (5.38)$$

and

$$\begin{aligned} F_{mc}^{qq} = & M_1e_3^2S^2 + M_2(e_4^2 + e_5^2)S^2 + M_3(4e_1e_2 - e_6^2)S^2 + M_4(e_1 + e_2)e_3S^2 \\ & + M_5((e_1 - e_2)e_4 + e_5e_6)S^2 + M_6(2e_1^2 + 2e_2^2 + e_6^2)S^2, \end{aligned} \quad (5.39)$$

where K_1, K_2 are linear-quadratic (LQ) constants and M_1, M_2, M_3, M_4, M_5 , and M_6 are quadratic-quadratic (QQ) constants. Minimizing the total free energy $F(e, S)$ (5.34) with respect to strains gives six equations:

$$\frac{\partial F}{\partial e_\alpha} = 0 \quad \text{for } \alpha = 1, \dots, 6. \quad (5.40)$$

Neglecting the quadratic-quadratic coupling, solutions for the system of equations (5.40) in terms of the spin polarization S correspond to

$$\begin{aligned} e_1 &= \frac{(K_1C_{33} - K_2C_{13})S^2}{-2C_{13}^2 + (C_{11} + C_{12})C_{33}} \\ e_2 &= \frac{(K_1C_{33} - K_2C_{13})S^2}{-2C_{13}^2 + (C_{11} + C_{12})C_{33}} \\ e_3 &= -\frac{S^2(K_2C_{11} + K_2C_{12} - 2K_1C_{13})}{-2C_{13}^2 + (C_{11} + C_{12})C_{33}} \\ e_4 &= 0 \\ e_5 &= 0 \\ e_6 &= 0 \end{aligned} \quad (5.41)$$

The strains e_1, e_2 and e_3 exhibit a linear temperature dependence (like S^2 - see solutions 5.33). As the strain $e_1 = e_2$ with $e_4 = e_5 = e_6 = 0$, these solutions indicate that the

magnetoelastic coupling does not change the crystal's symmetry. Other terms, such as the coupling between the spins and the soft mode might account for the observed symmetry change at low temperatures. The total free energy (5.34) can also be used to calculate the elastic constants using (4.16). The elastic constants for this current model with both linear-quadratic and quadratic-quadratic magnetoelastic coupling are listed in Table 5.1. We note from Table 5.1 that the number of independent elastic constants is unchanged. Again, this indicates that there is no symmetry change associated with the magnetoelastic coupling. We also see that, the model predicts a jump at T_{N1} ($S=0$) for the elastic constants that depend on the linear-quadratic coupling constants K_i . As the experimental observations for C_{ij} do not exhibit any discontinuity at T_{N1} , we can consider that the linear-quadratic coupling coefficients are small and we thus set $K_1 = K_2 = 0$.

5.2.1 Numerical model calculation and its prediction

In order to make contact with experimental data, the temperature scale of the spin order parameter, as defined in equation (5.33), has been rescaled in order to coincide with the anomalies observed on the ultrasound data presented in chapter 4. Let us first analyze the temperature dependence of the velocity of longitudinal modes propagating along the z-direction. This mode is particularly interesting as, according to the non-spin model presented in chapter 4 (see Fig. 4.3 c), the coupling with the soft mode is weak. At the same time, the prediction associated with the spin polarization, Table 5.1, indicates that $\frac{\Delta V_{Lz}}{V_{Lz}} \sim \frac{1}{2} \cdot \frac{\Delta C_{33}}{C_{33}}$ should be proportional to S^2 . Thus, we compare in Fig. 5.4 the temperature dependence of $\frac{\Delta V_{Lz}}{V_{Lz}}$ with that of the square of the spin polarization as given by equation (5.33). In that Fig., the experimental results are represented by black continuous line while the mean field prediction corresponds to the red continuous line. We immediately note that critical phenomena is significant at low temperatures. In order to obtain a more realistic prediction, we also present in Fig. 5.4 a non-mean field calculation (see continuous blue line), by replacing the mean-field critical exponent $\beta = 0.5$ with $\beta = 0.3$ (close to Ising universality), where

Table 5.1: Effective elastic constants for both phases of CuFeO_2 as a function of S .

Elastic Constant	Trigonal ($R\bar{3}m$)	Monoclinic ($C/2m$)
C_{11}	C_{11}^o	$C_{11}^o - \frac{K_1^2}{2C_Q} + 4M_6S^2$
C_{12}	C_{12}^o	$C_{12}^o - \frac{K_1^2}{2C_Q} + 4M_3S^2$
C_{13}	C_{13}^o	$C_{13}^o - \frac{K_1K_2}{2C_Q} + 4M_4S^2$
C_{14}	C_{14}^o	$C_{14}^o + M_5S^2$
C_{24}	$-C_{14}^o$	$-C_{14}^o - M_5S^2$
C_{33}	C_{33}^o	$C_{33}^o - \frac{K_2^2}{2C_Q} + 2M_1S^2$
C_{44}	C_{44}^o	$C_{44}^o + 2M_2S^2$
C_{66}	C_{66}^o	$C_{66}^o + 2(-M_3 + M_6)S^2$

Table 5.2: Values of coupling constants (LQ and QQ)

K_1	K_2	M_1	M_2	M_6
0	0	2.4×10^9	1.1×10^7	1.1×10^9

$S \sim (T_N - T)^\beta$. This value seems reasonable as we obtain a good agreement with the experimental data. All proportional constants used for comparison in the present calculations are given in Table 5.2.

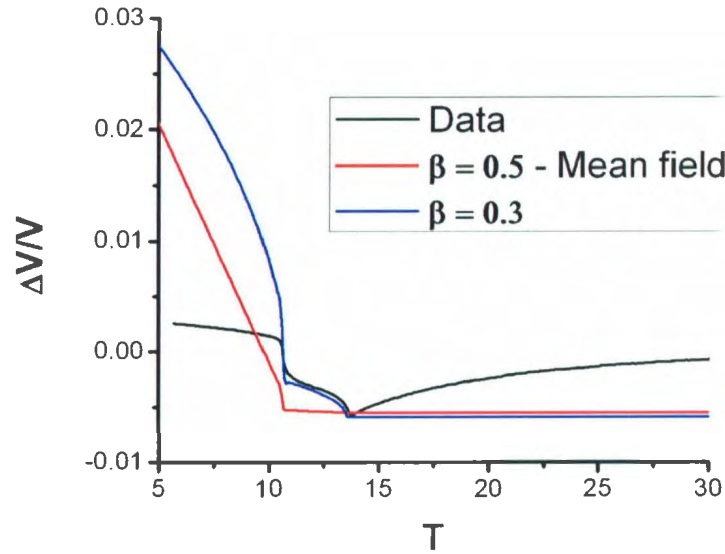


Figure 5.4: Normalized Velocity Plot: $\Delta V_{Lz}/V_{Lz}$. Red curve represents the mean field result and blue curve represents the non-mean field.

We now focus our attention on the effect of the magnetic coupling on the velocity of longitudinal and transverse modes propagating along the y-direction (V_{Ly} and V_{TyPz}). For those particular modes, shown in Fig. 4.3 (a) and (d), it is clear that the coupling with the soft mode associated with the structural phase transition must also be taken

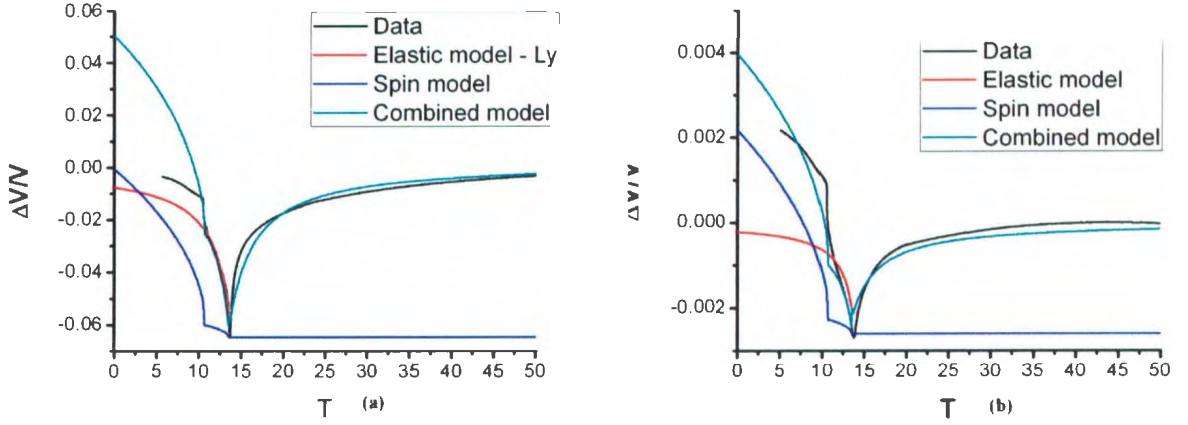


Figure 5.5: Normalized Velocity Plots: (a) $\Delta V_{Ly}/V_{Ly}$, (b) $\Delta V_{TyPz}/V_{TyPz}$ - We are using a different scale for each plot in order to show the good compatibility of the model and data fit.

into consideration. To clearly illustrate the relative weight of both contributions, we present in Fig. 5.5 each contribution separately. Thus, in Fig. 5.5, the experimental data are again represented by a black continuous line while the contributions associated with the spin and the soft mode are illustrated by a blue, and red continuous line, respectively. In this Fig. 5.5, the coupling constants M_1 and M_2 given in Table 5.2 have been adjusted in order to reproduce the amplitude of the discontinuity observed at T_{N2} . Moreover, the spin contribution presented here correspond to a non-mean field calculation using $\beta = 0.3$ as determine in Fig. 5.4. In Fig. 5.5, the continuous green line represents the combined model, which includes both soft and spin contribution. It shows good agreement with experimental results. Our analysis indicates that magnetoelastic effects principally account for anomalies observed on the velocity measurements below T_{N2} while those observed around T_{N1} are dominated by the coupling with a soft mode.

Chapter 6

Conclusions

In this thesis, we study the temperature dependence of the elastic properties of the magnetoelectric compound CuFeO_2 near structural and magnetic phase transitions using various Landau model free energies. The results of this analysis are compared to the experimental ultrasonic velocity measurements provided by Dr. G. Quirion at Memorial University.

In the first part of this thesis work, we investigated the elastic properties of this compound, in the neighborhood of the magnetic and structural phase transitions near 14 K. The temperature ranges in our investigation was 4 K - 50 K. Dr. Quirion's high resolution sound velocity measurement show that CuFeO_2 undergoes two phase transitions at $T_{N1} = 13.7$ K and $T_{N2} = 10.6$ K, respectively. We derived a theoretical model to explain these experimental results. In the high-temperature rhombohedral $R\bar{3}m$ phase, we observed that the elastic constant C_{66} shows a strong softening, while C_{11} and C_{44} show less softening. These experimental results agrees with our assumptions and numerical predictions derived from the model. The softening behavior on C_{66} is large and non-linear. Therefore, we can conclude from our study that the structural transition at T_{N1} is categorized as pseudo-proper ferroelastic. The observed structural phase transition corresponds to $R\bar{3}m \rightarrow C2/m$ symmetry change. Using the ultrasonic sound velocity measurements, we obtained the temperature dependence of the independent elastic constants of CuFeO_2 .

In the last part of this thesis work, we analyzed the impact of magnetoelastic coupling. A Landau model free energy which depends only on magnetic degrees of freedom (spin density) shows that there are two magnetic phase transitions at $T_{N1} = 1.08$ and $T_{N2} = 0.85$ in units of near-neighbour exchange coupling J_1 . A Landau model free energy containing spin, elastic, and magnetoelastic coupling was analyzed. We obtained the temperature dependence of three of the six independent elastic constants of CuFeO_2 due to spin-lattice effects. We found that the transition at T_{N2} is first order. For the moment we don't have experimental results to figure out the exact values of the interaction quantities J_1 , J_2 , J_3 and J' . However, we conclude that our current rescaled theoretical results agree with the experimental data for C_{ij} . We also reproduce the amplitude of the discontinuity observed in three principal modes at T_{N2} , which we could not explain with the soft modes only. Our study shows that the anomalies at T_{N1} are dominated by the coupling with a soft mode while the anomalies at T_{N2} are correlated to the spin polarization. Thus, we conclude that magnetoelastic coupling is strongly impacting the elastic properties of CuFeO_2 and that this results in magneto-electric coupling [7].

Our theoretical studies are based on a Landau model free energy which was developed from symmetry arguments. We found good numerical predictions consistent with the temperature dependence of the measured ultrasonic sound velocity modes. However, our current theoretical model is not complete. For a complete quantitative analysis, we need to expand our Landau model free energy, constructed from the symmetry arguments, to include coupling between spin polarization (S) and the structural order parameter (Q). This would then lead to a free energy with a multitude of terms involving e , Q and S : $F = F_e + F_Q + F_S + F_{eQ} + F_{eS} + F_{QS}$, where F_e , F_Q and F_S , are elastic, structural Landau, spin energies and F_{eQ} , F_{eS} and F_{QS} are coupling involving strain and the structural order parameter, strain and the spin polarization, and spin polarization and the structural order parameter respectively.

Bibliography

- [1] G. Quirion, M.J. Tagore, M.L. Plumer and O.A. Petrenko, *Phys. Rev. B* **77**, 094111 (2008).
- [2] M. Fiebig, *J. Phys. D* **38**, R123 (2005).
- [3] W. Prellier, M. P. Singh and P. Murugavel, *J. Phys. Condens. Matter* **17**, R803 (2005).
- [4] X. Chen et al, *Appl. Phys. Lett.* **89**, 202508 (2006).
- [5] C. T. Prewitt, R. D. Shannon, and D. B. Rogers, *Inorg. Chem.* **10**, 791 (1971).
- [6] S. Mitsuda, H. Yoshizawa, N. Yaguchi, and M. Mekata, *J. Phys. Soc. Japan* **60**, 1885 (1991); M. Mekata, N. Yaguchi, T. Takagi, T. Sugino, S. Mitsuda, H. Yoshizawa, N. Hosoita and T. Shinojo, *J. Phys. Soc. Japan* **62**, 4474 (1993).
- [7] T. Kimura, J. C. Lashley, and A. P. Ramirez, *Phys. Rev. B* **73**, 220401(R) (2006).
- [8] O. A. Petrenko, G. Balakrishnan, M. R. Lees, D. McK. Paul and A. Hoser, *Phys. Rev. B* **62**, 8983 (2000); O. A. Petrenko, M. R. Lees, G. Balakrishnan, S. de Brion and G. Chouteau, *J. Phys. Condens. Matter* **17**, 2741 (2005).
- [9] W. M. Xu, M. P. Pasternak and R. D. Taylor, *Phys. Rev. B* **69**, 052401 (2004).
- [10] S. Mitsuda, N. Kasahara, T. Uno and M. Mase, *J. Phys. Soc. Japan* **67**, 4026 (1998).
- [11] K. Aizu, *J. Phys. Soc. Japan* **28**, 706 (1970).
- [12] E. Dieulesaint and D. Royer, *Elastic Waves in Solids: Applications to Signal Processing* (John Wiley & Sons Inc, 1980).
- [13] M.J.P. Musgrave, *Crystal Acoustics* (Holden-Day, Inc, 1985).
- [14] Charles Kittel, *Introduction to Solid State Physics* (John Wiley & Sons, Inc, 2005).

- [15] Jean-Claude Tolédano and Pierre Tolédano, *The Landau Theory of Phase Transitions* (World Scientific, 1987), Vol. 3.
- [16] Ekhard K. H. Salje, *Phase Transitions in Ferroelastic and Co-Elastic Crystals* (Cambridge University Press, 1983).
- [17] Gerald Burns, *Solid State Physics* (Academic Press, Inc, 1985).
- [18] N. Terada, Y. Tanaka, Y. Tabata, K. Katsumata, A. Kikkawa and S. Mitsuda, *J. Phys. Soc. Japan* **75**, 113702 (2006).
- [19] F. Ye, Y. Ren, Q. Huang, J. A. Fernandez-Baca, P. Dai, J. W. Lynn and T. Kimura, *Phys. Rev. B* **73**, 220404(R) (2006).
- [20] S. Kojima, *J. Phys. Condens. Matter.* **10**, L327 (1998).
- [21] P. Rocquet and M. Couzi, *J. Phys. C: Solid State Phys.* **18**, 6571 (1985); A Gomez-Cuevas, J. M. Perez-Mato, E. H. Bocanegra, M. Couzi and J. P. Chaminade, *J. Phys. C: Solid State Phys.* **21**, 3641 (1988).
- [22] M. Sepiarsky, M. G. Stachiotti and R. L. Migoni, *Phys. Rev. B* **56**, 566 (1997).
- [23] P. Tolédano, M. M. Fejer, B. A. Auld, *Phys. Rev. B* **27**, 5717 (1983).
- [24] M. J. Harris, D. F. McMorrow and K. W. Godfrey, *Phys. Rev. Lett.* **79**, 4846 (1997).
- [25] B. Mróz, H. Kiefte, M. J. Clouter and J. A. Tuszyński, *J. Phys. Condens. Matter* **5**, 6377 (1993).
- [26] K. Knorr, A. Loidi and J. K. Kjems, *Phys. Rev. Lett.* **55**, 2445 (1985).
- [27] G. Quirion, W. Wu, J. Rideout, and B. Mróz, [arxiv:cond-mat/pdf/0606064](https://arxiv.org/abs/cond-mat/0606064) (unpublished).
- [28] B. Mróz, H. Kiefte, M. J. Clouter and J. A. Tuszyński, *Phys. Rev. B* **43**, 641 (1991).
- [29] S. C. Abrahams, *Mat. Res. Bull.* **6**, 881 (1971).
- [30] Michael Tinkham, *Group Theory and Quantum Mechanics* (Dover Publications Inc, 1964).
- [31] Yu. A. Freiman and H. J. Jodl, *Phys. Rep.* **401**, 1 (2004).

- [32] S. Mitsuda, M. Mase, K. Prokes, H. Kitazawa, and H. A. Katori, *J. Phys. Soc. Japan* **69**, 33 (2000).
- [33] M. L. Plumer and A. Caillé, *Phys. Rev. B* **37**, 7712 (1988).
- [34] M. Whangbo, K. Lee, R. K. Kremer, *Chem. Mater.* **18**, 1268 (2006).
- [35] M. L. Plumer, (To be published).
- [36] M. L. Plumer, *Phys. Rev. B* **76**, 144411 (2007).

